Site dilution of quantum spins in the honeycomb lattice

Eduardo V. Castro,[1,2] N. M. R. Peres,[1,3,4] K. S. D. Beach[1], and Anders W. Sandvik[1]
[1] *Department of Physics, Boston University, 590 Commonwealth Avenue, Boston, MA 02215, USA*
[2] *CFP and Departamento de Física, Faculdade de Ciências, Universidade do Porto, P-4169-007 Porto, Portugal*
[3] *Max-Planck-Institut für Physik komplexer Systeme, Nöthnitzer Str. 38, 01187 Dresden, Germany and*
[4] *Center of Physics and Departamento de Física, Universidade do Minho, P-4710-057, Braga, Portugal*
(Dated: August 8, 2005)

We discuss the effect of site dilution on both the magnetization and the density of states of quantum spins in the honeycomb lattice, described by the antiferromagnetic Heisenberg spin-S model. Since the disorder introduced by the dilution process breaks translational invariance, the model has to be solved in real space. For this purpose a real-space Bogoliubov-Valatin transformation is used. In this work we show that for the $S > 1/2$ the system can be analyzed in terms of linear spin wave theory, in the sense that for all dilution concentrations the assumptions of validity for the theory hold. For spin $S = 1/2$, however, the linear spin wave approximation breaks down. In this case, we have studied the effect of dilution on the staggered magnetization using the Stochastic Series Expansion Monte Carlo method. Two main results are to be stressed from the Monte Carlo method: (i) a better value for the staggered magnetization of the undiluted system, $m_{\rm av}(L \to \infty) = 0.2677(6)$, relatively to the only result available to date in the literature, and based on Trotter error extrapolations; (ii) a finite value of the staggered magnetization of the percolating cluster at the classical percolation threshold, showing that there is no quantum critical transition driven by dilution in the Heisenberg model. In the solution of the problem using linear the spin wave method we pay special attention to the presence of zero energy modes. We show, for a finite-size system (in a bipartite lattice), that if the two sub-lattices are evenly diluted the system always has two zero energy modes, which play the role of Goldstone boson modes for a diluted lattice, having no translation symmetry but supporting long range magnetic order. We also discuss the case when the two sub-lattices are not evenly diluted. In this case, for finite size lattices, the Goldstone modes are not a well defined concept, and special care is needed in taking them into account in order for sensible physical results can be obtained. Using a combination of linear spin wave analysis and the recursion method we were able to obtain the thermodynamic limit behavior of the density of states for both the square and the honeycomb lattices. We have used both the staggered magnetization and the density of states to analyze neutron scattering experiments (determining the effect of dilution on the system's magnetic moment) and Néel temperature measurements on quasi-two-dimensional honeycomb systems. Our results are in quantitative agreement with experimental results on $Mn_pZn_{1-p}PS_3$ (a diluted $S = 5/2$ system) and on the $Ba(Ni_pMg_{1-p})_2V_2O_8$ (a diluted $S = 1$ system). Our work should stimulate further experimental research in Heisenberg diluted-honeycomb systems.

PACS numbers: 75.10.Jm, 75.50.Ee, 75.30.Ds, 75.40.Mg

I. INTRODUCTION

The study of dilution and its effect on the magnetic properties of antiferromagnetic materials is a central problem in modern condensed matter theory.[1–5] For the square lattice, a number of important experimental and theoretical results have been reported.[1,3–5] For the honeycomb lattice, there are some experimental results in the literature[2] already, but the corresponding theoretical understanding lags far behind.

Insulating antiferromagnets are possible candidates for exhibiting quantum critical points separating ordered from disordered phases. The quantum corrections to the staggered magnetization of diluted antiferromagnetic insulators became an important experimental and theoretical topic after site dilution of La_2CuO_4 by non magnetic impurities,[1,6] such as Zn or Mg. Theoretical studies interpreting the magnetic properties of these diluted systems have been recently performed,[3–5,7] showing a good agreement between theory and experiment. A description of the effect of dilution on the spin flop phase of La_2CuO_4 was attempted from the point of view of a simple mean field theory,[8] with some qualitative agreement with experimental results. In addition, the expectation of a magnetic quantum phase transition driven by the interplay of dilution and quantum fluctuations was shown not to occur in the antiferromagnetic Heisenberg model in a square lattice.[4,5] In the undiluted case, on the other hand, it was shown that the Heisenberg model itself is incapable of describing the high energy part of the spin wave spectrum; a calculation starting from the Hubbard model was shown to give the correct high energy behavior.[9–11]

The key role played by dimensionality in determining

the behavior of a system of quantum magnetic moments lends special importance to the honeycomb lattice, which has the lowest possible co-ordination in more than one dimension (see Fig. 1). Realizations of insulating antiferromagnets based on this lattice have already been achieved both with and without magnetic dilution. Recently Spremo *et al.*[12] have studied the magnetic properties of a metal-organic antiferromagnet on an undiluted but distorted honeycomb lattice. The authors found good agreement between the theoretical predictions obtained within the framework of a modified spin wave approach and the experimental results for the magnetization as a function of uniform external field and for the uniform zero-field susceptibility.

Honeycomb layers are also found in transition-metal thiophosphates MPS_3, where M is a first row transition metal. These compounds are viewed as "perfect" 2D magnetic systems because of the weak van der Waals cohesion energy binding the layers. In each layer the magnetic ions are arranged in a honeycomb lattice. Neutron diffraction and magnetic susceptibility studies on $MnPS_3$, $FePS_3$, and $NiPS_3$ antiferromagnets[13–15] ($S = 5/2$, $S = 2$, and $S = 1$, respectively) showed the existence of quite different types of ordering among the different compounds. Whereas for $FePS_3$ and $NiPS_3$ the metal ions are coupled ferromagnetically to two of the nearest neighbors and antiferromagnetically to the third, for $MnPS_3$ all nearest neighbors interactions within a layer are antiferromagnetic. In fact, it turns out that the simplest nearest-neighbor antiferromagnetic Heisenberg model is a reasonable approximation for the description of the magnetic properties in $MnPS_3$, although the second- (J_2) and third-nearest-neighbor (J_3) interactions—which are both also antiferromagnetic—are not negligible for this compound ($J_1/J_2 \sim 10$ and $J_1/J_3 \sim 4$).[16] Substitution of magnetic Mn^{2+} ions by nonmagnetic Zn^{2+} impurities showed that long-range order (LRO) is lost at $p = 0.46 \pm 0.03$ for $Mn_pZn_{1-p}PS_3$.[2,17,18] The fact that LRO is preserved for dilutions higher than the classical percolation threshold for the honeycomb lattice, $p_c \simeq 0.7$, is attributed to the significance of J_2 and J_3 in this compound.

Recently, Rogado *et al.*[19] have characterized the magnetic properties of the $S = 1$ honeycomb compound $BaNi_2V_2O_8$, which can be described as a weakly anisotropic 2D Heisenberg antiferromagnet.[20] The magnetic Ni^{2+} ions lie on weakly coupled honeycomb layers, exhibiting antiferromagnetic LRO close to 50 K. The doped compound $Ba(Ni_pMg_{1-p})_2V_2O_8$ has a fraction $1 - p$ of the honeycomb layer sites substituted by Mg^{2+}—a nonmagnetic ion. Magnetic susceptibility studies showed that the Néel temperature is substantially reduced with increasing doping in the range $0.84 \leq p \leq 1$. For $p = 0.84$ the onset of antiferromagnetic LRO occurs only at $T_N \simeq 17$ K, a T_N reduction of almost 70% relative to its undiluted value. It would be interesting to know whether the suppression of antiferromagnetic LRO by nonmagnetic impurities occurs at the classical percolation transition $p_c \simeq 0.7$, as predicted by our calculations (see below).

In addition to these exciting experimental results, the theoretical result of Mucciolo *et al.* for the square lattice,[4] where the vanishing of the staggered magnetization for the $S = 1/2$ systems coincides with the classical percolation transition, opened the naive expectation that for a 2D lattice with nonfrustrating nearest neighbor interactions and a smaller number of neighbors, magnetic quantum-phase transitions driven by the interplay of disorder and quantum fluctuations could occur. The honeycomb lattice is the simplest realization of such a lattice, for its coordination number is smaller than that of the square lattice. On the other hand, large-scale quantum Monte Carlo simulations of the square lattice have shown that the percolating cluster actually has a robust long-range order,[5] in disagreement with the spin wave calculation where this order vanishes very close to the percolation point. Hence, spin wave theory is not reliable at and close to the percolation point for $S = 1/2$, and we expect this break-down also for the honeycomb lattice at the percolation point. This expectation is confirmed; we have performed quantum Monte Carlo simulations that show only a rather modest reduction of the sublattice magnetization of the percolating cluster, whereas there is no long-range order in spin wave theory for $S = 1/2$ in this case.

Experimental $S = 1/2$ antiferromagnetic systems with honeycomb lattice structure have already been reported by Zhou *et al.*[21] in the A_2CuBr_4 salt, where A is morpholinium ($C_4H_{10}NO$). Their data is well described by a nearest-neighbor antiferromagnetic Heisenberg model, but with two different couplings J_a and J_b. To the best of our knowledge, the dilution of this system has not yet been attempted.

Motivated by the experimental results on diluted $Mn_pZn_{1-p}PS_3$ and $Ba(Ni_pMg_{1-p})_2V_2O_8$ and by the possibility of quantum phase transitions driven by the interplay of disorder and quantum fluctuations, we study here the effect of site dilution on the magnetic properties of the Heisenberg antiferromagnetic nearest-neighbor model, for an arbitrary spin-S value. Our study is performed both at zero and finite temperatures. A first attempt to understand the effect of a nonmagnetic defect on the properties of the $S = 1/2$ 2D Heisenberg antiferromagnet in the honeycomb lattice was made by de Châtel *et al.*[22] In their mean-field approach, a single impurity was introduced in clusters up to 12 spins. It is clear, however, that their results can only be applied to systems with dilutions up to $1-p = 1/13$. Moreover, the random nature of defects cannot be accounted for using their method.

In this paper, we follow the general idea of the work of Mucciolo *et al.*,[4] by using the linear spin wave approximation in real space to compute different physical quantities. In addition we use finite-size scaling to determine the magnetic moment of the samples. We address the problem of determining the density of states (DOS)

of our system using a different and more reliable method, which gives the behavior of the DOS in the thermodynamic limit. The paper is organized as follows: in Sect. II we present the Hamiltonian and the formalism we use; in Sect. III we give the numerical details of our method; we present the results on the staggered magnetization and on density of states as well as on the cluster characterization in Sect. IV; finally, in Sect. V we summarize our work and present some concluding remarks.

II. MODEL HAMILTONIAN AND FORMALISM

The Heisenberg Hamiltonian describing quantum spins in a site-diluted honeycomb lattice is written as

$$H = J \sum_{i\in A,\boldsymbol{\delta}} \eta_i \eta_{i+\boldsymbol{\delta}} \mathbf{S}_i^a \cdot \mathbf{S}_{i+\boldsymbol{\delta}}^b \,, \tag{1}$$

where $\mathbf{S}_i^a$ ($\mathbf{S}_i^b$) is the spin operator on a site i of sublattice A (B). The notation $i+\boldsymbol{\delta}$ represents a nearest neighbor site of site i, connected to i by the vector $\boldsymbol{\delta}$. There are three different $\boldsymbol{\delta}$ vectors given by

$$\boldsymbol{\delta}_1 = \frac{c}{2}(1,\sqrt{3})\,, \quad \boldsymbol{\delta}_2 = \frac{c}{2}(1,-\sqrt{3})\,, \quad \boldsymbol{\delta}_3 = -c(1,0)\,, \tag{2}$$

where c is the hexagon side length. The η_i variables can have the values 0 or 1 depending on whether the site i exists or not.

The usual spin wave approximation starts by assuming that LRO exists and, in the case of antiferromagnetism, that the ground state is not substantially different from the Néel state. The mathematical meaning of this similarity is that the following inequalities should hold:

$$S - \left\langle S_i^{a,z} \right\rangle \ll S \quad \text{for } i \in A, \tag{3}$$

$$S + \left\langle S_i^{b,z} \right\rangle \ll S \quad \text{for } i \in B. \tag{4}$$

With these in mind we express the spin operators in terms of bosonic creation and annihilation operators as introduced by Holstein and Primakoff.[23] Holstein-Primakoff transformation is defined for sublattice A as

$$\begin{aligned} S_i^{a,z} &= S - a_i^\dagger a_i \,, \\ S_i^{a,+} &= \sqrt{2S}\sqrt{1-\frac{a_i^\dagger a_i}{2S}}\, a_i \,, \\ S_i^{a,-} &= \sqrt{2S}\, a_i^\dagger \sqrt{1-\frac{a_i^\dagger a_i}{2S}} \,. \end{aligned} \tag{5}$$

In sublattice B the spin have $S_z = -S$ projection in the Néel state. Since the bosons should describe excitations above the ground state, and this has to be such that inequalities (3) and (4) are verified, the $S^{b,z}$ operator needs to be redefined as $S_i^{b,z} = -S + b_i^\dagger b_i$. Accordingly, the $S_i^{b,+}$ operator must create bosons, and all the operators in sublattice B are defined as

$$\begin{aligned} S_i^{b,z} &= -S + b_i^\dagger b_i \,, \\ S_i^{b,-} &= \sqrt{2S}\sqrt{1-\frac{b_i^\dagger b_i}{2S}}\, b_i \,, \\ S_i^{b,+} &= \sqrt{2S}\, b_i^\dagger \sqrt{1-\frac{b_i^\dagger b_i}{2S}} \,. \end{aligned} \tag{6}$$

It is worth mentioning that inequalities (3) and (4) can also be expressed in terms of the new bosonic operators a and b as

$$\left\langle a_i^\dagger a_i \right\rangle \ll S \quad \text{for } i \in A, \tag{7}$$

$$\left\langle b_i^\dagger b_i \right\rangle \ll S \quad \text{for } i \in B, \tag{8}$$

from which the linear spin wave approximation follows straightforwardly by expanding the square roots in Eqs. (5) and (6) in powers of $1/S$ and keeping only the zeroth order terms:

$$\begin{aligned} S_i^{a,+} &\simeq \sqrt{2S}\, a_i \,, \quad & S_i^{b,-} &\simeq \sqrt{2S}\, b_i \,, \\ S_i^{a,-} &\simeq \sqrt{2S}\, a_i^\dagger \,, \quad & S_i^{b,+} &\simeq \sqrt{2S}\, b_i^\dagger \,, \end{aligned} \tag{9}$$

Inserting the resultant approximation (9) into Eq. (1) produces the linear spin wave Hamiltonian, which reads

$$\begin{aligned} H = &-Jh_a S(S+1) \sum_{i\in A,\boldsymbol{\delta}} \eta_i \eta_{i+\boldsymbol{\delta}} \\ &+ JS \sum_{i\in A,\boldsymbol{\delta}} \eta_i \eta_{i+\boldsymbol{\delta}} \Big[h_a \big(a_i a_i^\dagger + b_{i+\boldsymbol{\delta}}^\dagger b_{i+\boldsymbol{\delta}} \big) \\ &\qquad + a_i b_{i+\boldsymbol{\delta}} + b_{i+\boldsymbol{\delta}}^\dagger a_i^\dagger \Big] \,. \end{aligned} \tag{10}$$

Note that we have introduced a magnetic anisotropy h_a in the $S_i^{a,z} S_{i+\boldsymbol{\delta}}^{b,z}$ term.

The linear spin wave Hamiltonian (10) can be seen as having a classical part of the form

$$H_{\rm cl} = -Jh_a S(S+1) \sum_{i\in A,\boldsymbol{\delta}} \eta_i \eta_{i+\boldsymbol{\delta}} \,, \tag{11}$$

and a quantum fluctuating part, which can be written as

$$H_{\rm sw} = (\{a\},\{b^\dagger\}) \mathbf{D} (\{a\},\{b^\dagger\})^\dagger \,, \tag{12}$$

where $(\{a\},\{b^\dagger\})^\dagger$ is a column vector containing all the boson operators and

$$\mathbf{D} = \begin{pmatrix} \mathbf{K}^a & \boldsymbol{\Delta} \\ \boldsymbol{\Delta}^T & \mathbf{K}^b \end{pmatrix} \tag{13}$$

is the so-called grand dynamical matrix. For a diluted lattice, the number of sites in sublattice A need not be the same as that in sublattice B; therefore the dimensions of the blocks in $\mathbf{D}$ are $N_a \times N_a$ for $\mathbf{K}^a$, $N_b \times N_b$ for $\mathbf{K}^b$,

$N_a \times N_b$ for $\mathbf{\Delta}$ and $N_b \times N_a$ for $\mathbf{\Delta}^T$. The corresponding matrix elements are

$$K^a_{ij} = Jh_a S\delta_{ij}\eta_i \sum_{\boldsymbol{\delta}} \eta_{i+\boldsymbol{\delta}}\,, \qquad \text{for } i \in A, \tag{14}$$

$$K^b_{ij} = Jh_a S\delta_{ij}\eta_i \sum_{\boldsymbol{\delta}} \eta_{i+\boldsymbol{\delta}}\,, \qquad \text{for } i \in B, \tag{15}$$

$$\Delta_{ij} = JS\eta_i\eta_j\,, \qquad \text{for } i \in A,\, j \in i+\boldsymbol{\delta}, \tag{16}$$

$$\Delta^T_{ij} = JS\eta_i\eta_j\,, \qquad \text{for } i \in B,\, j \in i+\boldsymbol{\delta}. \tag{17}$$

The diagonalization of the bosonic Hamiltonian amounts to find a transformation $\mathbf{T}$ such that

$$(\mathbf{T}^\dagger)^{-1}\mathbf{D}\mathbf{T}^{-1} = \mathrm{diag}(\omega_1,\ldots,\omega_{N_a},\omega_{N_a+1},\ldots,\omega_{N_a+N_b})\,, \tag{18}$$

where $\mathrm{diag}(\omega_1,\ldots,\omega_{N_a+N_b})$ stands for a diagonal matrix with elements $\omega_1,\ldots,\omega_{N_a+N_b}$ in its diagonal, $N_a + N_b$ in number. In this case all the eigenvalues $\omega_1,\ldots,\omega_{N_a},\omega_{N_a+1},\ldots,\omega_{N_a+N_b}$ are positive. The quasi-particles associated with those eigenvalues are obtained from

$$(\{\alpha\},\{\beta^\dagger\})^\dagger = \mathbf{T}(\{a\},\{b^\dagger\})^\dagger\,. \tag{19}$$

In the undiluted case, it is well known that Eq. (12) can be diagonalized through a Bogoliubov-Valatin transformation in the reciprocal space. For a subsequent analysis it is convenient to reproduce here the results of the calculation for the undiluted honeycomb lattice.[24] We first introduce the operators $a_{\mathbf{k}}$ and $b_{\mathbf{k}}$ defined as the inverse Fourier transforms of a_i and b_i,

$$a_i = \frac{1}{\sqrt{N_a}}\sum_{\mathbf{k}} e^{-i\mathbf{k}\cdot\mathbf{r}_i}a_{\mathbf{k}}\,, \quad b_i = \frac{1}{\sqrt{N_b}}\sum_{\mathbf{k}} e^{-i\mathbf{k}\cdot\mathbf{r}_i}b_{\mathbf{k}}\,, \tag{20}$$

where the $\mathbf{k}$ summation ranges over the first Brillouin zone of either sublattice A or B. (Do not confuse the site index i and the complex imaginary unit also present in the Fourier transform). The vector $\mathbf{r}_i$ is the position vector of site i, and $N_a = N_b$ in the absence of dilution. Substituting Eq. (20) into Hamiltonian (12) gives us $H_{\mathrm{sw}} = \sum_{\mathbf{k}} H_{\mathbf{k}}$, with

$$H_{\mathbf{k}} = JSz\Big[h_a\big(a_{\mathbf{k}}a^\dagger_{\mathbf{k}} + b^\dagger_{-\mathbf{k}}b_{-\mathbf{k}}\big) + \phi_{\mathbf{k}}a_{\mathbf{k}}b_{-\mathbf{k}} + \phi^*_{\mathbf{k}}b^\dagger_{-\mathbf{k}}a^\dagger_{\mathbf{k}}\Big], \tag{21}$$

where $\phi_{\mathbf{k}}$ is defined as

$$\phi_{\mathbf{k}} = \frac{1}{z}\sum_{\boldsymbol{\delta}} e^{-i\mathbf{k}\cdot\boldsymbol{\delta}}\,. \tag{22}$$

The diagonalized form of Hamiltonian (21), given by

$$H_{\mathbf{k}} = \omega_{\mathbf{k}}\big(1 + \alpha^\dagger_{\mathbf{k}}\alpha_{\mathbf{k}} + \beta^\dagger_{\mathbf{k}}\beta_{\mathbf{k}}\big)\,, \tag{23}$$

with

$$\omega_{\mathbf{k}} = JSz\sqrt{h_a^2 - |\phi_{\mathbf{k}}|^2}, \tag{24}$$

can be easily obtained from the following Bogoliubov-Valatin transformation,

$$\begin{aligned}\alpha_{\mathbf{k}} &= u_{\mathbf{k}}a_{\mathbf{k}} + v_{\mathbf{k}}b^\dagger_{-\mathbf{k}}\,,\\ \beta_{\mathbf{k}} &= v_{\mathbf{k}}a^\dagger_{\mathbf{k}} + u_{\mathbf{k}}b_{-\mathbf{k}}\,,\end{aligned} \tag{25}$$

with coefficients $u_{\mathbf{k}}$ and $v_{\mathbf{k}}$ given as functions of the parameters h_a and $\phi_{\mathbf{k}}$.

In the diluted case, translational symmetry is lost, and the solution in the reciprocal space is as difficult as the one in real space. Let us start by constructing an operator transformation of the Bogoliubov-Valatin type in real space which can be used in the presence of dilution:

$$\alpha_n = \sum_{i=1}^{N_a} u_{ni}a_i + \sum_{i=1}^{N_b} v_{ni}b^\dagger_i\,, \tag{26}$$

$$\beta_n = \sum_{i=1}^{N_a} w_{ni}a^\dagger_i + \sum_{i=1}^{N_b} x_{ni}b_i\,. \tag{27}$$

This definition of $\alpha^\dagger$ and $\beta^\dagger$ excitations gives us N_a α-type quasi-particles and N_b β-type quasi-particles. Equations (26) and (27) define the transformation matrix (19),

$$\mathbf{T} = \begin{pmatrix}\mathbf{U}^* & \mathbf{V}^*\\ \mathbf{W} & \mathbf{X}\end{pmatrix}, \tag{28}$$

where the $N_a\times N_a$ ($N_b\times N_a$) and $N_a\times N_b$ ($N_b\times N_b$) matrices $\mathbf{U}^*$ ($\mathbf{W}$) and $\mathbf{V}^*$ ($\mathbf{X}$) contain the coefficients u^*_{ni} (w_{ni}) and v^*_{ni} (x_{ni}), respectively. Since the quasi-particles must have a bosonic character, the quasi-particle operators must satisfy the commutation relations

$$\big[\alpha_n,\alpha^\dagger_m\big] = \big[\beta_n,\beta^\dagger_m\big] = \delta_{nm}\,, \tag{29}$$

$$\big[\alpha_n,\beta_m\big] = \big[\beta^\dagger_n,\alpha^\dagger_m\big] = 0\,, \tag{30}$$

which lead to the following constraints on the transformation coefficients:

$$\sum_{i=1}^{N_a} u_{ni}u^*_{mi} - \sum_{i=1}^{N_b} v_{ni}v^*_{mi} = \delta_{nm}\,, \tag{31}$$

$$\sum_{i=1}^{N_a} w_{ni}w^*_{mi} - \sum_{i=1}^{N_b} x_{ni}x^*_{mi} = -\delta_{nm}\,, \tag{32}$$

$$\sum_{i=1}^{N_a} u_{ni}w_{mi} - \sum_{i=1}^{N_b} v_{ni}x_{mi} = 0\,, \tag{33}$$

$$\sum_{i=1}^{N_a} w^*_{ni}u^*_{mi} - \sum_{i=1}^{N_b} x^*_{ni}v^*_{mi} = 0\,. \tag{34}$$

Equations (31–34) can be written in matrix notation as

$$\mathbf{U}\mathbf{U}^\dagger - \mathbf{V}\mathbf{V}^\dagger = \mathbf{U}^*\mathbf{U}^T - \mathbf{V}^*\mathbf{V}^T = \mathbf{I}_{N_a}\,, \tag{35}$$

$$\mathbf{W}\mathbf{W}^\dagger - \mathbf{X}\mathbf{X}^\dagger = \mathbf{W}^*\mathbf{W}^T - \mathbf{X}^*\mathbf{X}^T = -\mathbf{I}_{N_b}\,, \tag{36}$$

$$\mathbf{U}\mathbf{W}^T - \mathbf{V}\mathbf{X}^T = \mathbf{W}\mathbf{U}^T - \mathbf{X}\mathbf{V}^T = \mathbf{0}\,, \tag{37}$$

$$\mathbf{W}^*\mathbf{U}^\dagger - \mathbf{X}^*\mathbf{V}^\dagger = \mathbf{U}^*\mathbf{W}^\dagger - \mathbf{V}^*\mathbf{X}^\dagger = \mathbf{0}\,, \tag{38}$$

where $\mathbf{I}_{N_a}$ ($\mathbf{I}_{N_b}$) is the $N_a \times N_a$ ($N_b \times N_b$) unit matrix. These relations can be put into a more compact form by defining the matrix

$$\mathbf{1}_p = \begin{pmatrix} \mathbf{I}_{N_a} & \mathbf{0} \\ \mathbf{0} & -\mathbf{I}_{N_b} \end{pmatrix}, \tag{39}$$

in terms of which Eqs. (35–38) can be rewritten as

$$\mathbf{T}\mathbf{1}_p\mathbf{T}^\dagger = \mathbf{1}_p\,. \tag{40}$$

Since $\mathbf{1}_p\mathbf{1}_p = \mathbf{I}_{N_a+N_b}$, it can be shown, after simple algebraic transformations, that

$$\mathbf{T}^\dagger\mathbf{1}_p\mathbf{T} = \mathbf{1}_p\,. \tag{41}$$

As a result we have four additional (though not independent) sets of orthogonality equations,

$$\sum_{n=1}^{N_a} u_{ni}u^*_{nj} - \sum_{n=1}^{N_b} w^*_{ni}w_{nj} = \delta_{ij}\,, \tag{42}$$

$$\sum_{n=1}^{N_a} v_{ni}v^*_{nj} - \sum_{n=1}^{N_b} x^*_{ni}x_{nj} = -\delta_{ij}\,, \tag{43}$$

$$\sum_{n=1}^{N_a} v_{ni}u^*_{nj} - \sum_{n=1}^{N_b} x^*_{ni}w_{nj} = 0\,, \tag{44}$$

$$\sum_{n=1}^{N_a} u_{ni}v^*_{nj} - \sum_{n=1}^{N_b} w^*_{ni}x_{nj} = 0\,. \tag{45}$$

Since transformations (26) and (27) diagonalize the spin wave Hamiltonian (12), the quasi-particles will obey the following commutation relations:

$$[\alpha_n, H_{\rm sw}] = \omega^{(\alpha)}_n\alpha_n\,, \tag{46}$$

$$[\beta_n, H_{\rm sw}] = \omega^{(\beta)}_n\beta_n\,, \tag{47}$$

$$\left[\alpha^\dagger_n, H_{\rm sw}\right] = -\omega^{(\alpha)}_n\alpha^\dagger_n\,, \tag{48}$$

$$\left[\beta^\dagger_n, H_{\rm sw}\right] = -\omega^{(\beta)}_n\beta^\dagger_n\,. \tag{49}$$

[Notice that we have relabeled the positive eigenvalues introduced in (18) to $\omega^{(\alpha)}_1, \ldots, \omega^{(\alpha)}_{N_a}, \omega^{(\beta)}_1, \ldots, \omega^{(\beta)}_{N_b}$.] From Eqs. (46) and (26) we can define an eigenvalue matrix equation in the usual form, namely,

$$\begin{pmatrix} \mathbf{K}^a & -\mathbf{\Delta} \\ \mathbf{\Delta}^T & -\mathbf{K}^b \end{pmatrix} \begin{pmatrix} \bar{u}_n \\ \bar{v}_n \end{pmatrix} = \omega^{(\alpha)}_n \begin{pmatrix} \bar{u}_n \\ \bar{v}_n \end{pmatrix}, \tag{50}$$

where the column vectors $\bar{u}_n$ and $\bar{v}_n$ contain the coefficients u_{ni} and v_{ni}, respectively. From Eq. (49) and the complex conjugate of Eq. (27), a similar eigenvalue matrix equation can be defined,

$$\begin{pmatrix} \mathbf{K}^a & -\mathbf{\Delta} \\ \mathbf{\Delta}^T & -\mathbf{K}^b \end{pmatrix} \begin{pmatrix} \bar{w}^*_n \\ \bar{x}^*_n \end{pmatrix} = -\omega^{(\beta)}_n \begin{pmatrix} \bar{w}^*_n \\ \bar{x}^*_n \end{pmatrix}. \tag{51}$$

Defining the matrices

$$\mathbf{\Omega}_\alpha = \mathrm{diag}(\omega^{(\alpha)}_1, \ldots, \omega^{(\alpha)}_{N_a})\,, \tag{52}$$

and

$$\mathbf{\Omega}_\beta = \mathrm{diag}(\omega^{(\beta)}_1, \ldots, \omega^{(\beta)}_{N_b})\,, \tag{53}$$

and recalling definition (28) for $\mathbf{T}$ and definition (39) for $\mathbf{1}_p$, Eqs. (50) and (51) can be combined into a single equation,

$$\mathbf{D}\mathbf{1}_p\mathbf{T}^\dagger = \mathbf{T}^\dagger \begin{pmatrix} \mathbf{\Omega}_\alpha & \mathbf{0} \\ \mathbf{0} & -\mathbf{\Omega}_\beta \end{pmatrix}. \tag{54}$$

This can be made more compact still by defining the matrix $\mathbf{\Omega} = \mathrm{diag}(\omega^{(\alpha)}_1, \ldots, \omega^{(\alpha)}_{N_a}, \omega^{(\beta)}_1, \ldots, \omega^{(\beta)}_{N_b})$, such that

$$\mathbf{D}\mathbf{1}_p\mathbf{T}^\dagger = \mathbf{T}^\dagger\mathbf{\Omega}\mathbf{1}_p\,. \tag{55}$$

From Eq. (55) and the relations (40) and (41), it is not difficult to show that

$$\mathbf{1}_p\mathbf{T}\mathbf{1}_p\mathbf{D}\mathbf{1}_p\mathbf{T}^\dagger\mathbf{1}_p = \mathbf{\Omega}\,. \tag{56}$$

Thus, solving the eigenvalue problem defined by Eq. (54) under the constraint (40) is equivalent to finding a transformation $\mathbf{T}$ which satisfies Eq. (18), and where, obviously,

$$\mathbf{1}_p\mathbf{T}^\dagger\mathbf{1}_p = \mathbf{T}^{-1}\,. \tag{57}$$

According to Eq. (19), the diagonalized form of the spin wave Hamiltonian is obtained as

$$\begin{aligned} H_{\rm sw} &= (\{a\}, \{b^\dagger\})\mathbf{D}(\{a\}, \{b^\dagger\})^\dagger \\ &= (\{\alpha\}, \{\beta^\dagger\})\mathbf{\Omega}(\{\alpha\}, \{\beta^\dagger\})^\dagger \\ &= \sum_{n=1}^{N_a} \omega^{(\alpha)}_n\alpha_n\alpha^\dagger_n + \sum_{n=1}^{N_b} \omega^{(\beta)}_n\beta^\dagger_n\beta_n\,. \end{aligned}$$

The conclusion of the above discussion is that the operator transformation given by Eqs. (26) and (27) diagonalizes the spin wave Hamiltonian (10) and that $\alpha^\dagger$ and $\beta^\dagger$ are the quasi-particles (with bosonic character) associated with the low energy excitations of the antiferromagnetic Heisenberg Hamiltonian for quantum spins in a site diluted honeycomb lattice (needless to say the above description applies to other lattices as well).

Using Eq. (19) it is possible to write any average of the initial bosonic operators in terms of the quasi-particle operators α and β. The simplest example is the staggered magnetization $M^{\rm stagg}_z$ at $T = 0$ given by

$$\begin{aligned} M^{\rm stagg}_z &= \left\langle \sum_{i\in A} S^{a,z}_i - \sum_{i\in B} S^{b,z}_i \right\rangle \\ &= \big(N_a + N_b\big)\big(S - \delta m_z\big)\,, \end{aligned} \tag{58}$$

where

$$\delta m_z = \sum_{n=1}^{N_a} \delta m^{(n,\alpha)}_z + \sum_{n=1}^{N_b} \delta m^{(n,\beta)}_z\,, \tag{59}$$

with

$$\delta m_z^{(n,\alpha)} = \frac{1}{N_a + N_b} \sum_{i \in B} |v_{ni}|^2 \,, \tag{60}$$

and

$$\delta m_z^{(n,\beta)} = \frac{1}{N_a + N_b} \sum_{i \in A} |w_{ni}|^2 . \tag{61}$$

III. NUMERICAL DETAILS

The formalism developed in the above section is based on the existence of the matrix $\mathbf{T}$ and, naturally, on the possibility of finding it by some numerical procedure. In this work we have used two independent methods to compute the transformation matrix and the associated eigenenergies. Both methods agree with each other within the numerical accuracy of the calculation. One of them is based on a Cholesky decomposition and gives the $\mathbf{T}^{-1}$ matrix directly, whereas the other solves the eigenvalue problem defined by Eq. (54), computing the matrix $\mathbf{T}^\dagger$ and from this the matrix $\mathbf{T}$.

A. Cholesky Decomposition method

As shown by Colpa,[25] so long as the grand dynamical matrix is positive definite, a simple algorithm exists for determining $\mathbf{T}$. A hermitian (or symmetric) matrix is positive definite if all its eigenvalues are positive. By definition the quasi-particles $\alpha^\dagger$ and $\beta^\dagger$ have positive or zero excitation energy. As will be shown in Subsect. III C, the zero energy excitations are associated with spin rotations, which cost zero energy due to the spin rotational symmetry of the isotropic Heisenberg model. So, provided that $h_a \geq 1^+$, all eigenvalues are positive and the grand dynamical matrix is positive definite. The algorithm is implemented in three major steps:

1. for $\mathbf{D}$ positive definite a Cholesky decomposition can be performed[26] and we have $\mathbf{D} = \mathbf{Q}\mathbf{Q}^\dagger$, where $\mathbf{Q}$ is an upper triangular matrix. The existence of a Cholesky decomposition guarantees that the problem is positive definite;

2. it can be proved that there exists a unitary transformation $\mathbf{Y}$ such that $\mathbf{Y}^\dagger(\mathbf{Q}\mathbf{1}_p^{(ab)}\mathbf{Q}^\dagger)\mathbf{Y} = \mathbf{1}_p^{(ab)}\,\mathrm{diag}(\omega_1, \ldots, \omega_{N_a}, \omega_{N_a+1}, \ldots \omega_{N_a+N_b})$;

3. finally, it can be proved that $\mathbf{T}^{-1} = \mathbf{Q}^{-1}\mathbf{Y}\,\mathrm{diag}(\sqrt{\omega_1}, \ldots, \sqrt{\omega_{N_a+N_b}})$.

B. Bogoliubov-Valatin Transformation method

The nonhermitian eigenproblem defined by Eq. (54) can be solved with standard numerical algorithms. Here we have used subroutines of the LAPACK library. It should be noted that the resultant eigenvectors do not provide the required $\mathbf{T}^\dagger$ matrix directly. After diagonalization the eigenvectors have to be normalized such that they satisfy Eqs. (31) and (32) for $n = m$. Degenerate eigenvectors[53] have to be carefully analyzed because the LAPACK subroutines we have used do not guarantee that they satisfy Eq. (40) (though Eqs. (31) to (34) are satisfied by default for $n \neq m$). The algorithm is implemented as follows:

1. the matrix $\mathbf{D}\mathbf{1}_p^{(ab)}$ is reduced to an upper Hessenberg form $\mathbf{H}$ by an orthogonal transformation $\mathbf{Y}$, *i.e.*, $\mathbf{H} = \mathbf{Y}\mathbf{D}\mathbf{1}_p^{(ab)}\mathbf{Y}^\dagger$ (LAPACK subroutines DGEHRD and DORGHR);

2. the eigenvalues of the upper Hessenberg matrix (the same as those of $\mathbf{D}\mathbf{1}_p^{(ab)}$) and the matrices $\mathbf{Q}$ and $\mathbf{Z}$ from the Schur decomposition $\mathbf{H} = \mathbf{Z}\mathbf{Q}\mathbf{Z}^\dagger$, where $\mathbf{Q}$ is an upper quasi-triangular matrix (the Schur form), and $\mathbf{Z}$ is the orthogonal matrix of Schur vectors, are computed (LAPACK subroutine DHSEQR);

3. the right eigenvectors of the upper quasi-triangular matrix $\mathbf{Q}$ are computed and multiplied by $\mathbf{Y}^\dagger\mathbf{Z}$,[54] giving the right eigenvectors of $\mathbf{D}\mathbf{1}_p^{(ab)}$, whose matrix form we name $\widetilde{\mathbf{T}}^\dagger$ (LAPACK subroutines DTREVC);

4. degenerate column eigenvectors of $\widetilde{\mathbf{T}}^\dagger$ are arranged in linear combinations such that they satisfy Eq. (40);

5. nondegenerate column eigenvectors of $\widetilde{\mathbf{T}}^\dagger$ are normalized so as to satisfy the orthogonality relations of Eqs. (31) and (32), giving matrix $\mathbf{T}^\dagger$;

6. the positive eigenvalues and respective eigenvectors are identified with α modes, and the negative ones with the β modes;

7. eigenvalues and eigenvectors are sorted such that matrix $\mathbf{T}^\dagger$ has the form defined in Eq. (28).

C. Zero modes

It is well known that the clean and isotropic limit of Hamiltonian (10) has two zero-energy excitations (Goldstone bosons), whose momenta can be determined from Eq. (23). These gapless modes are a consequence of the fact that the ground state spontaneously breaks the rotational symmetry of the Hamiltonian in spin space. It can be shown[27] that these zero-energy modes have divergent amplitudes. In two and three dimensions the quantum corrections to the staggered magnetization (at zero temperature) are finite, meaning that the divergence associated with the zero energy modes is integrable. We

note, however, that if the mean square amplitudes of the differences between the two x- and y-components, given by

$$\frac{1}{N_a+N_b}\left(\sum_{i\in A} S_i^{a,x} - \sum_{i\in B} S_i^{b,x}\right) \tag{62}$$

and

$$\frac{1}{N_a+N_b}\left(\sum_{i\in A} S_i^{a,y} - \sum_{i\in B} S_i^{b,y}\right), \tag{63}$$

are computed, we immediately find divergent behavior.[28] The same divergent behavior is also found if we try to get the staggered magnetization (58) from a finite-size scaling procedure, doing summations in $\mathbf{k}$-space for finite-size systems, including all momenta of the Brillouin zone.

As shown by Anderson,[27,28] this does not mean that the spin wave approximation is breaking down and that the system has no LRO. What it means is that these divergences are related to the zero point motion of the Goldstone modes, and their presence is required to exist since in a finite-size system one cannot have solutions that break the spin rotational symmetry of the problem.[29] The presence of a *broken symmetry ground state* is made possible if we analyze the $H_{\mathbf{0}}$ term in Eq. (21), from which the Goldstone modes arise. This term cannot be diagonalized through any Bogoliubov-Valatin transformation. Actually, it has a continuum spectrum starting from the zero energy ground state (see Appendix A). Using this continuum of states we can form a wave packet centered around some prefixed orientation in spin space, with the property of having both a finite staggered magnetization, and a mean square roots of the quantities (62) and (63) scaling with $1/N^{\frac{1}{2}-\alpha}$, with $\alpha > 0$, as long as we pay some extra energy. In addition, it can be shown (see Appendix B) that this extra energy scales as $1/N^{\frac{1}{2}+\alpha}$, being negligible in the thermodynamic limit. Thus it is a suitable approximation to form the above mentioned wave packet from the solutions of $H_{\mathbf{0}}$, and to study the energy and the zero point motion of all other normal modes within a time interval smaller than that needed for the zero-energy wave packet to disrupt the coherence of the unidirectional state.[27] The understanding of the role played by Goldstone bosons in finite-size systems is crucial for computing well defined quantities in the thermodynamic limit from calculations in finite-size lattices. As a practical example, the staggered magnetization can be obtained from the finite-size calculations if the Goldstone zero point motion contributions are subtracted, because the $H_{\mathbf{0}}$ solutions were already used to form the starting broken symmetry state. From this procedure we get exactly the same value as from the convergent integral in the continuum limit.

The above discussion now needs to be carried on to the diluted case, where the above aspects are more delicate than in the nondisordered case. In the presence of dilution, it is easy to verify that there is at least one zero mode in Eq. (50) in the isotropic case. This nontrivial solution with zero energy satisfies the equation

$$\begin{pmatrix} \mathbf{K}^a & -\mathbf{\Delta} \\ \mathbf{\Delta}^T & -\mathbf{K}^b \end{pmatrix}\begin{pmatrix} \bar{c} \\ \bar{c} \end{pmatrix} = 0, \tag{64}$$

with all the amplitudes constant. To prove that this is indeed an eigenstate we only need to remember definitions (14–17) of matrices $\mathbf{K}^a$, $\mathbf{K}^b$ and $\mathbf{\Delta}$, and check that the following equalities always hold:

$$K_{ii}^a = \sum_{j=N_a}^{N_a+N_b} \Delta_{ij}\,, \tag{65}$$

$$K_{ii}^b = \sum_{j=1}^{N_a} \Delta_{ij}^T\,. \tag{66}$$

In terms of quasi-particle excitations, the eigenvector defined by Eq. (64) can be expressed as[55]

$$\alpha_0^\dagger \propto \sum_{i=1}^{N_a} a_i^\dagger + \sum_{i=1}^{N_b} b_i\,, \tag{67}$$

in the case of an α-type excitation, and

$$\beta_0^\dagger \propto \sum_{i=1}^{N_a} a_i + \sum_{i=1}^{N_b} b_i^\dagger\,, \tag{68}$$

if it is a β-type excitation. Recalling the approximate expressions in Eq. (9) for the operators $S_i^{(a,b)+}$ and $S_i^{(a,b)-}$ in terms of bosonic operators a and b, Eqs. (67) and (68) can be rewritten as

$$\alpha_0^\dagger \propto S_{\rm tot}^-\,, \tag{69}$$

$$\beta_0^\dagger \propto S_{\rm tot}^+\,. \tag{70}$$

Thus, excitations $\alpha_0^\dagger$ and $\beta_0^\dagger$ are precisely the Goldstone bosons associated with the broken continuous symmetry of spin rotation in the diluted system.

As will be shown in Subsect. III E, the thermodynamic limit of the staggered magnetization for the diluted system will be obtained from a finite-size scaling analysis. As we have started from a broken symmetry ground state (the wave packet), which is a direct consequence of Eqs. (3) and (4), we would proceed as in the clean limit and neglect the contributions of α_0 and β_0 modes. However, although in the undiluted case the number of Goldstone modes is always two, when dilution is present this number can either be one or two, in a finite size lattice. The reason why this is so is that operators $S_{\rm tot}^-$ and $S_{\rm tot}^+$ do not always represent independent excitations, *i.e.*, they do not always commute. Naturally $S_{\rm tot}^-$ and $S_{\rm tot}^+$ never commute strictly speaking because

$$[S_{\rm tot}^+, S_{\rm tot}^-] = 2S_{\rm tot}^z\,. \tag{71}$$

Nevertheless, in the clean limit we can easily convince ourselves that the expectation value of $S^z_{\rm tot}$ is always zero, and, as $S^z_{\rm tot}$ is a constant of the motion, commutator (71) will always be zero. To get the value of the commutator (71) in the presence of dilution we make use of Eq. (9), from which one finds

$$[S^+_{\rm tot}, S^-_{\rm tot}] \propto N_a - N_b \,. \tag{72}$$

Now it is easily seen that one can have one or two Goldstone modes in a finite-size diluted system: if the number of undiluted sites in each sublattice is the same ($N_a = N_b$) there will be two Goldstone modes; otherwise, if $N_a \neq N_b$, there will be only one. Applying to this case the reasoning used for the undiluted case, we should then neglect the contributions of the existent Goldstone modes.

As the system size increases, the fluctuations relative to the zero mean value of $N_a - N_b$ should scale as $1/\sqrt{N_a + N_b}$, statistically speaking. Therefore the difference $N_a - N_b$ is again zero in the thermodynamic limit and the system has two zero energy excitations. This situtation cannot be achieved in finite size lattices, unless we restrict ourselvess to cases where the disordered realizations are constrained to obey the condition $N_a = N_b$, being clear that the staggered magnetization in the thermodynamic limit cannot depend on this restriction. We stress, however, that without this restriction the conclusions drawn from finite-size lattices would be different if we had accepted all sorts of disordered lattice realizations. This difference is due to the contribution of the "quasi-divergent" energy modes that emerge when $N_a \neq N_b$. We will get back to this point in Sect. IV, presenting numerical evidence for what we have just analysed.

D. Cluster formation and periodic boundary conditions

The study of diluted lattices requires the concept of *largest cluster*, and therefore some care is required in constructing the effective lattice where the quantum problem is to be solved. Since we are interested in dilution, the algorithms discussed in Subsecs. III A and III B are to be implemented not on all occupied lattice sites, but only on the sites defined by the largest connected cluster of spins, since in the thermodynamic limit a finite magnetization cannot exist if one is below the percolation critical threshold $p_{\rm c}$. The dilution is induced in the lattice by diluting any site with probability $1 - p$. For $p = 1$ there is no dilution at all. When $p = p_{\rm c}$ a classical percolation transition occurs in the thermodynamic limit preventing the existence of magnetic long range order in the system. According to Suding and Ziff,[30] $p_{\rm c} = 0.697043(3)$ in the honeycomb lattice. Here we use $p_{\rm c} = 0.697043$.

We work with finite size lattices where periodic boundary conditions (p.b.c.) are implemented as defined in Fig. 1. In Fig. 1 the links on the border are labeled according to which site they connect to. The lattices are characterized by their linear dimension L ($L = 3$ in Fig. 1). The total number of sites for a given L is $2L^2$.

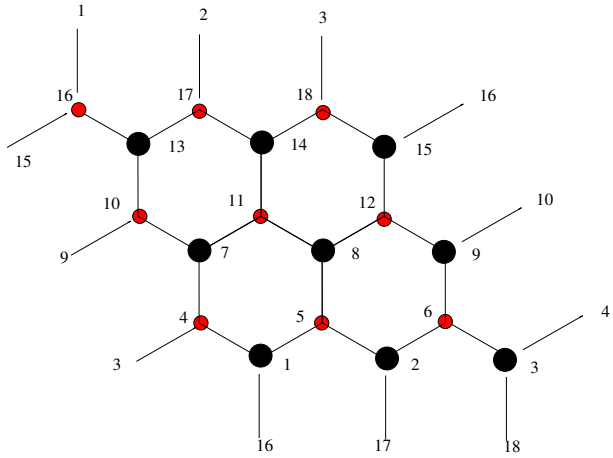

FIG. 1: (color online) A finite size honeycomb lattice showing the periodic boundary conditions used in the numerical calculations.

The algorithm starts by identifying the largest cluster, for rigid boundary conditions (this is, with no p.b.c.). As in Ref. 4, it is only after the largest cluster is found that we apply p.b.c. to the original lattice, checking whether there are new sites belonging to the largest cluster. As previously discussed in Subsect. III C, only clusters with $N_a = N_b$ are to be used, so we reject all disordered lattice realizations in which $N_a \neq N_b$.[56] Finally, the eigenvalue problem is solved for the final cluster using the aforementioned algorithms. In Fig. 2 we show an example of a disorder realization and the corresponding cluster labeling process at $p = p_{\rm c}$. The larger cluster found for rigid boundary conditions can be seen in panel (**c**) of Fig. 2. After p.b.c. implementation the final cluster has a larger number of elements (panel (**d**) in Fig. 2).

E. Finite-size scaling

The eigenvalue problem determines all the eigenvalues and eigenfunctions for the cluster, and from these the corrections to the staggered magnetization are computed according to Eq. (59). For a given p value, $N_{\rm rz}$ disordered lattice realizations with $N_a = N_b$ are performed, leading to an average staggered magnetization density $m_{\rm av}$

$$m_{\rm av}(p, L) = \frac{1}{N_{\rm rz}} \sum_{i=1}^{N_{\rm rz}} \frac{M_z^{{\rm stagg},i}}{N_m^i} \,, \tag{73}$$

where $M_z^{{\rm stagg},i}$ is the value of Eq. (58), and N_m^i is the total number of magnetic (undiluted) sites in the lattice, for the given disorder realization i. Although $m_{\rm av}$ does not depend explicitly on L, the sizes of the clusters are

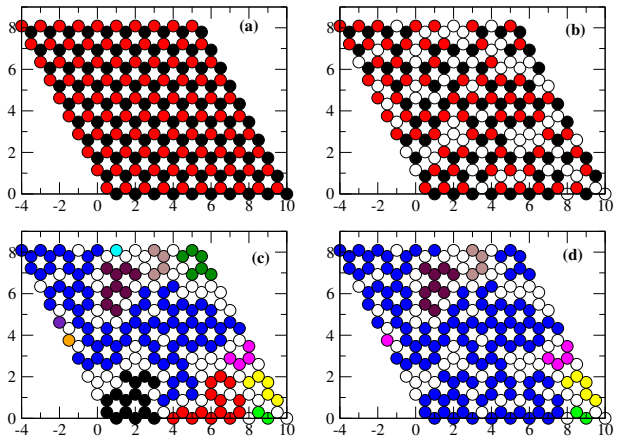

FIG. 2: (color online) An example, for a disorder realization in a lattice with $L = 10$, of the cluster formation. In **(a)** is the original lattice; in **(b)** each site is chosen to be diluted with probability $1 - p_c$ with $p_c = 0.697043$; in **(c)** the several (12 in this case) clusters with rigid boundary conditions have been determined; in **(d)** the larger cluster found in **(c)** is augmented by the periodic boundary conditions.

determined by L, and therefore different L's lead to different values for Eq. (73). With this definition we will be able to identify $m_{\rm av}(p, L \to \infty)$ with the ordered magnetic moment magnitude per magnetic ion measured in neutron diffraction experiments.

From Eq. (58) it is easily seen that $m_{\rm av}$ can be expressed as the average product of two different contributions, one purely classical ($m^i_{\rm cl}$) and the other purely quantum ($m^i_{\rm qm}$),

$$m_{\rm av}(p, L) = \frac{1}{N_{\rm rz}} \sum_{i=1}^{N_{\rm rz}} m^i_{\rm cl} m^i_{\rm qm} \,, \tag{74}$$

where we used the notation $m^i_{\rm cl} = \frac{N^i_c}{N^i_m}$ for the classical factor, with $N^i_c = N^i_a + N^i_b$, and $m^i_{\rm qm} = S - \delta m^i_z$ for the quantum mechanical factor. The quantum contribution is simply the staggered magnetization density of the larger cluster found in the disorder realization i. It would be S in the Néel state but it is reduced by $\delta m^i_z(p, L)$ due to quantum fluctuations, whose strength depend on dilution p and lattice size L. If LRO is present we can assume that the sublattice magnetization, or equivalently the staggered magnetization, is a self-averaging quantity, as was shown to happen in the square lattice case.[5] Thus, in the thermodynamic limit of $m_{\rm av}$ each disorder realization $m^i_{\rm qm}$ can then be replaced by its infinite-size-extrapolated average, which we denote by $m_{\rm qm}$,

$$m_{\rm av}(p, L \to \infty) = m_{\rm cl} m_{\rm qm} \,. \tag{75}$$

The classical factor now assumes the standard form for the order parameter of the classical percolation problem,

$$m_{\rm cl} = \left\langle \frac{N_c}{N_m} \right\rangle_{L\to\infty} \,, \tag{76}$$

which is zero for $p \le p_c$. Therefore a quantum critical point can only exist above p_c if $m_{\rm qm} = 0$ for some $p^* > p_c$. To find $m_{\rm qm}$ we need to compute the average infinite-size value of the quantum corrections δm^∞_z from our finite size calculations. We show that finite-size scaling can be found for this quantity, from which results holding in the thermodynamic limit can be obtained. In our study the size of the largest connected cluster $N_a + N_b$ is not fixed, instead the linear dimension of the lattice L is. As shown for the square lattice,[5] the alternative approach where the percolating cluster size is fixed leads to the same magnetization value in the thermodynamic limit. The finite-size scaling properties of the quantum correction to the magnetization are strictly not known for a disordered system at the percolation point. However, in practice a direct generalization of the pure-system scaling, using the fractal (Hausdorff) dimensionality, has been shown to work well.[5] Hence we will assume

$$\langle \delta m_z(p, L) \rangle_{N_{\rm rz}} = \delta m^\infty_z + a L^{-D/2} + b L^{-D} \,, \tag{77}$$

where δm^∞_z is the average quantum correction to the staggered magnetization density in the thermodynamic limit, and D is the fractal dimension of the cluster, which should have the universal value $D = 91/48$ at p_c (in two dimensions), as is confirmed for the square and triangular lattices.[31]

F. Density of states

The real space diagonalization procedure, either *Bogoliubov-Valatin* or *Cholesky decomposition*, is very time consuming, preventing us from accessing large clusters (in the honeycomb lattice $L = 16$ is our upper limit). Although for the staggered magnetization density a finite-size scaling analysis can be done, we cannot easily guess the thermodynamic limit behaviour of the DOS from results of systems as small as $L = 16$.

In this work the well known recursion method is used to compute the average DOS. With this method we can handle lattices as large as $L = 128$, with the advantage that the obtained DOS is not the typical finite size DOS of a system with $L = 128$, but instead a very good approximation for its thermodynamic limit value, guessed from this finite-size system. We refer the reader to the paper of R. Haydock[32] for details in the case of non-interacting fermionic systems. Being a real space method the effect of disorder can be easily incorporated. Here we adopt the formulation introduced in Ref. 33 for disordered electronic systems. Further details on the recursion method in relation to disordered bosonic bilinear systems [such as model Hamiltonian (12)] will be presented elsewhere.[34]

It is worth mentioning that the recursion method has proved to be a powerful technique even in the presence of interactions.[35] Actually, the continued fraction representation of the Fourier components of the one particle propagator, the basis of the recursion method, is also an

essential point in the Padé analytical continuation which usually arises in the many-body problem.[36]

We define the following set of zero temperature retarded Green's functions in the standard way,

$$\begin{aligned} G_{ij}^{ab}(t) &= -i\,\langle 0|\,\{a_i^\dagger(t), b_j^\dagger(0)\}\,|0\rangle\,\Theta(t), \\ G_{ij}^{ba}(t) &= -i\,\langle 0|\,\{b_i(t), a_j(0)\}\,|0\rangle\,\Theta(t), \\ G_{ij}^{aa}(t) &= -i\,\langle 0|\,\{a_i^\dagger(t), a_j(0)\}\,|0\rangle\,\Theta(t), \\ G_{ij}^{bb}(t) &= -i\,\langle 0|\,\{b_i(t), b_j^\dagger(0)\}\,|0\rangle\,\Theta(t), \end{aligned} \tag{78}$$

where the notation $|0\rangle$ is used for the ground state of the spin wave Hamiltonian (12). The Fourier components of each of the Green's functions in Eq. (78),

$$G_{ij}(E + i0^+) = \int_{-\infty}^{\infty} dt\, e^{i(E+i0^+)t} G_{ij}(t), \tag{79}$$

are the quantities of interest when determining the DOS. Defining the DOS as

$$\rho(E) = \frac{1}{N_\mathrm{c}}\left[\sum_{n=1}^{N_a}\delta(E-\omega_n^{(\alpha)}) + \sum_{n=1}^{N_b}\delta(E-\omega_n^{(\beta)})\right], \tag{80}$$

it can be easily shown that $\rho(E)$ is given in terms of the Fourier components of the Green's functions (79) as

$$\begin{aligned} \rho(E) = -\frac{1}{N_\mathrm{c}}\frac{1}{\pi}\mathrm{Im}\Bigg[&\sum_{i\in A} G_{ii}^{aa}(E+i0^+) \\ &- \sum_{i\in B} G_{ii}^{bb}(E+i0^+) - \sum_{i\in A} G_{ii}^{aa}(-E+i0^+) \\ &+ \sum_{i\in B} G_{ii}^{bb}(-E+i0^+)\Bigg]. \end{aligned} \tag{81}$$

The recursion method gives $\mathrm{Im}[G_{ij}(E+i0^+)]$ directly, the imaginary part of the Fourier components defined in Eq. (79),[34] from which the DOS is straightforwardly computed.

IV. RESULTS

A. Larger cluster statistics

The number of sites in a regular planar lattice goes as the square of its linear size. In the thermodynamic limit, the same scaling applies to the largest cluster of the corresponding randomly-site-diluted lattice. This behaviour persists up to the percolation threshold, at which point the lattice is dominated by a spanning cluster of *fractal* dimension. Beyond percolation, individual clusters are no longer extensive: they each constitute a vanishing fraction of the total number of sites.

For a honeycomb lattice of size L and dilution level $x = (1-p)/(1-p_\mathrm{c})$, let $P(N_\mathrm{c}|L,x)$ denote the probability that the largest cluster has N_c sites. The average size of the largest cluster is simply the corresponding first moment:

$$\bar{N}_\mathrm{c}(L,x) = \sum_{N_\mathrm{c}=1}^{2L^2} N_\mathrm{c} P(N_\mathrm{c}|L,x). \tag{82}$$

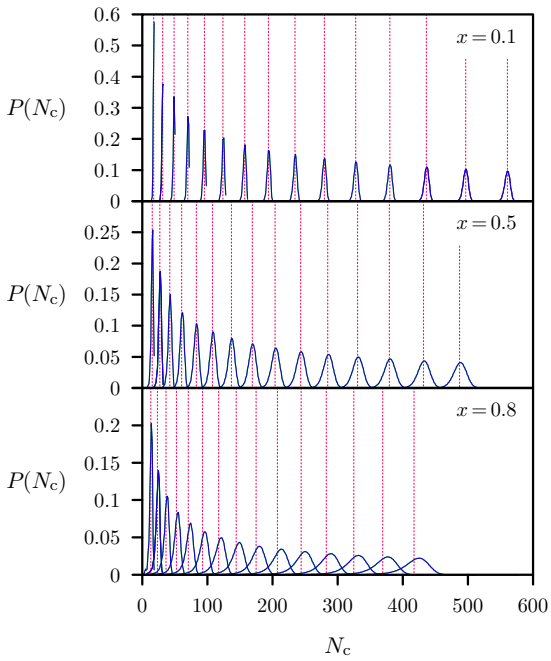

FIG. 3: (color online) The solid (blue) lines show the distribution of the number of sites in the largest cluster of a randomly site-diluted honeycomb lattice. From top to bottom, the three panels correspond to dilution levels $x = 0.1, 0.5, 0.8$. From left to right, the peaks correspond to linear system sizes $L = 4, 5, \ldots, 18$. The (red) vertical dotted lines indicated the average cluster sizes $\bar{N}_\mathrm{c}$, computed as per Eq. (82).

Example probability distributions for the honeycomb lattice are given in Fig. 3. For small x, the distributions are sharply peaked. As $x \to 1$, they become progressively broader and develop long tails skewed toward small values of N_c (marking the evolution to a different universal scaling function at percolation).

An effective scaling dimension $D_\mathrm{eff}(L,x)$ can be defined by the relation $\bar{N}_\mathrm{c} \sim L^{D_\mathrm{eff}}$. Its evolution with L is plotted in Fig. 4. Note that $D_\mathrm{eff}(L,x)$ has two points of attraction in the limit $L \to \infty$: $D_\mathrm{eff}(L, x<1) \to 2$ and $D_\mathrm{eff}(L,1) \to 91/48$. Plotted in the appropriate reduced coordinates—*viz.*, $L^D P(N_\mathrm{c})$ versus $L^{-D}N_\mathrm{c}$ where $D = 2$ below percolation and $D = 91/48$ at percolation—the probability distribution tends to either a simple delta function or the nontrivial curve shown in the inset of Fig. 4.

As can be seen in Fig. 4 (inset), a long tail is present for smaller cluster sizes. This enhancement of the larger cluster size distribution can be understood as a consequence

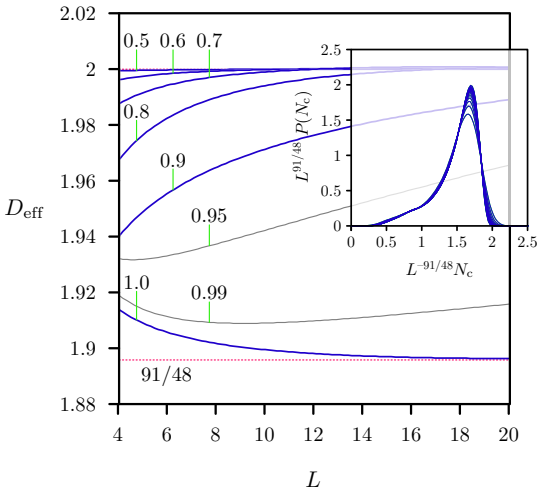

FIG. 4: (color online) The effective scaling dimension of the largest cluster takes one of two values in the $L \to \infty$ limit: $D_{\rm eff} = 2$ $(0 \le x < 1)$ or $D_{\rm eff} = 91/48$ $(x = 1)$. For $x \lesssim 0.5$, $D_{\rm eff}$ is close to its asymptotic value at all systems sizes. When x is close to 1, very large system sizes are necessary to reach the asymptotic regime. The figure inset shows the largest-cluster size distribution at percolation plotted in reduced coordinates. Each curve is computed as a histogram over 10^5 disorder realizations for system sizes $L = 5, 6, \ldots, 48$. As $L \to \infty$, the finite-size results converge to a smooth scaling function (one not dissimilar from that of the square-lattice case; see Fig. 2 of Ref. 5).

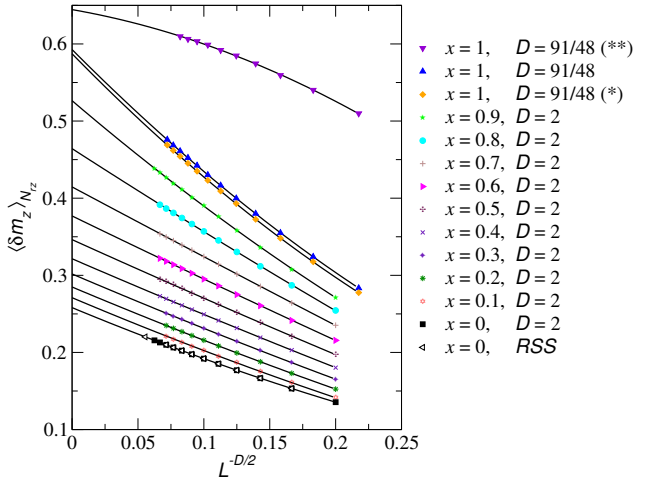

FIG. 5: (color online) Finite size scaling of $\langle \delta m_z \rangle$ for different values of $x = (1-p)/(1-p_c)$, obtained after 10^5 disorder realizations of lattices with equal number of sites in each sublattice. Also shown for $x = 1$ is the result obtained when the realized lattices are not constrained to have $N_a = N_b$: (*) zero modes were subtracted and the highest amplitude (nonzero) mode (see text) was subtracted if $N_a \neq N_b$; (**) only zero modes were subtracted. For $x = 0$ the *RSS* result was obtained by a *reciprocal space sum* using the analytical result.[24]

of the many possible disorder configurations for the same dilution. That is, we can have various smaller clusters instead of one large dominant cluster for the same number of diluted sites, though, of course, these disorder configurations are not so favorable.

B. Finite size scaling analysis

We have performed numerical real space diagonalization of model Hamiltonian (12), as described in Sect. III, for the honeycomb and the square lattices. Lattices with sizes $L = 5, 6, 7, 8, 9, 10, 11, 12, 13, 14, 15, 16$ (honeycomb) and $L = 6, 8, 10, 12, 14, 16, 18, 20, 22, 24, 26, 28$ (square) were generated. Averages were taken over $N_{\rm rz} = 10^5$ disorder realizations.[57]

In Figure 5 we show, for the honeycomb lattice, the average quantum correction to the staggered magnetization $\langle \delta m_z(p, L) \rangle_{N_{\rm rz}}$, for various values of dilution $x = (1-p)/(1-p_c)$, as a function of lattice size $L^{-D/2}$. The error bars are much smaller than the symbols used. The lines are fits to the points using the finite-size scaling hypotheses (77). The extrapolated zero abscissa value gives the average quantum correction to the staggered magnetization density in the thermodynamic limit $\delta m_z^{\infty}(p)$. In the undiluted case there is an excellent agreement between the real space diagonalization results (left-triangles) and the reciprocal space sum (black squares), obtained from the first **k**-summation in Eq. (C9) of Ref. 24, thus providing a reliability test to our algorithms.

For $p = p_c$ we show in Fig. 5 the results obtained from three different approaches. The blue up-triangles are the results of our standard technique discussed in Sect. III, *i.e.*, only lattices in which $N_a = N_b$ were considered and zero modes subtracted. The result labeled by violet down-triangles refers to a calculation in which the disordered realized lattices are not constrained to have $N_a = N_b$. The considerable difference between these two results is due to the presence of one "quasi-divergent" low energy (nonzero) mode when $N_a \neq N_b$. That is, even though we subtract the zero energy Goldstone mode as discussed in Sect. III for $N_a \neq N_b$, there is, in this situation, a low energy eigenstate that contributes in order $O(1)$ for δm_z, compared to the $O(1/N_c)$ contributions of the others eigenstates. If the contribution of this mode is subtracted the result labeled by orange diamonds is obtained, which agrees well with the result of our standard technique (where the constrain $N_a = N_b$ is always used).

To better understand the presence of this nonzero energy "quasi-divergent" mode when $N_a \neq N_b$, we have computed the contribution to δm_z from the lower nonzero energy mode $(\delta m_z^{(1)})$, and the next one in energy $(\delta m_z^{(2)})$, constrained to lattices with $N_a - N_b = \pm 1$. Figure 6 shows the behaviour of $\delta m_z^{(1)}$ (upper panel) and $\delta m_z^{(2)}$ (lower panel) with the average cluster size

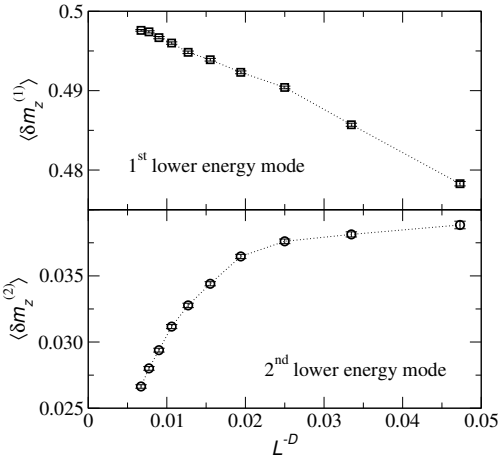

FIG. 6: Contributions to δm_z from: the lower nonzero energy mode (upper panel); the lower energy mode higher than the lower nonzero energy mode (lower panel). The average was taken over 10^4 disordered honeycomb lattices, with $N_a - N_b = \pm 1$, at $p = p_c$.

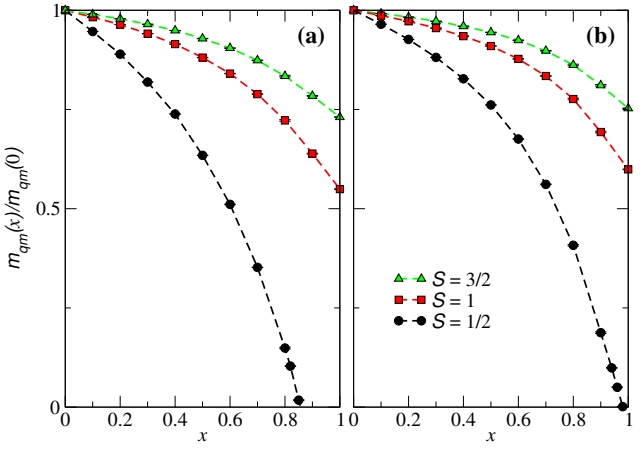

FIG. 7: (color online) Average quantum mechanical factor $m_{\rm qm}(x)$ vs dilution $x = (1-p)/(1-p_c)$ for different values of spin the S. Panel (**a**) shows the results for the honeycomb lattice and panel (**b**) for the square lattice.

$\bar{N}_c \propto L^D$. The $\delta m_z^{(2)}$ contribution decreases with $\bar{N}_c$, signaling the linear increase of the number of modes that contribute to δm_z. Instead, the contribution $\delta m_z^{(1)}$ increases with $\bar{N}_c$, and will be of $O(1)$ in the thermodynamic limit. As already mentioned in Sect. III, if N_a and N_b are both of magnitude 10^{23}, then, if $N_a - N_b = \pm 1$, there will be, for any practical purpose, two Goldstone modes and not only one. This statement should always be true if $|N_a - N_b| \ll N_a \sim N_b$. The results presented in top panel of Fig. 6 agree with this general picture. Furthermore, they imply that even for small sizes there is a mode, which will be identified with a Goldstone mode in the thermodynamic limit, that contributes "macroscopically" to δm_z, though having a finite energy.

C. Staggered magnetization

The results we found for the quantum mechanical factor $m_{\rm qm}(x)$ are summarized in Fig. 7 for the honeycomb lattice (panel (**a**)) and for the square lattice (panel (**b**)). Three different values of spin, $S = \frac{1}{2}, 1, \frac{3}{2}$, are shown.

In the undiluted limit we obtain $\delta m_z(0) \approx 0.258$ for the honeycomb lattice, and $\delta m_z(0) \approx 0.197$ for the square lattice. These results are in excellent agreement with quantum Monte Carlo results, namely, $\delta m_z(0) = 0.2323(6)$ for the spin 1/2 Heisenberg antiferromagnet in the honeycomb lattice (see Subsect. IV F), and $\delta m_z(0) = 0.1930(3)$ in the square lattice.[37]

The effect of the classical factor $m_{\rm cl}(x)$ (not shown) is only significant very close to p_c, where it vanishes with exponent 5/36.[38] Thus, for $S > \frac{1}{2}$ there is a classically driven order disorder transition at p_c. For $S = \frac{1}{2}$ linear spin wave theory predicts a *quantum critical point* in both the honeycomb and square lattices to occur at $x^* = 0.85(1)$ and $x^* = 0.98(1)$, respectively. Similar results for the square lattice were obtained in Ref. 4, though the limited number of averages over disorder prevented the authors to distinguish x^* from $x = 1$.

The predicted quantum critical point is absent in quantum Monte Carlo calculations, either in the honeycomb lattice or in the square lattice.[5] As already mentioned in Sect. II, we should not expect the validity of spin wave approximation when $\delta m_z \sim S$, because inequalities (7) and (8) break down in this situation. This is precisely what happens when disorder increases for $S = \frac{1}{2}$.

Comparison with experimental results

Now we compare our results for the staggered magnetization in the spin wave approximation with available experimental measurements on $Mn_pZn_{1-p}PS_3$ and $Ba(Ni_pMg_{1-p})_2V_2O_8$:

a. $Mn_pZn_{1-p}PS_3$ The layered compound $MnPS_3$ is a $S = 5/2$ Heisenberg antiferromagnet.[14] This huge spin value suggests that the spin wave approximation should work well in this case. Indeed, the average magnetic moment on the Mn atoms was found to be $4.5(2)\,\mu_B$ at 3.5 K in the pure material,[2] in excellent agreement with our spin wave result $m \approx 4.48\,\mu_B$. The effect of dilution in the average magnetic moment of Mn^{2+} ions is presented in Fig. 8. Neutron diffraction results on $Mn_pZn_{1-p}PS_3$ are shown as grey circles,[2] and the red squares are the theoretical results within the linear spin wave approximation. To go beyond p_c (the first-nearest neighbor percolation threshold) we would have to take into account second- and third-nearest neighbor couplings in Hamiltonian (1). Nevertheless, the effect of dilution for $p \leq p_c$ is already well described by the first-nearest neighbor

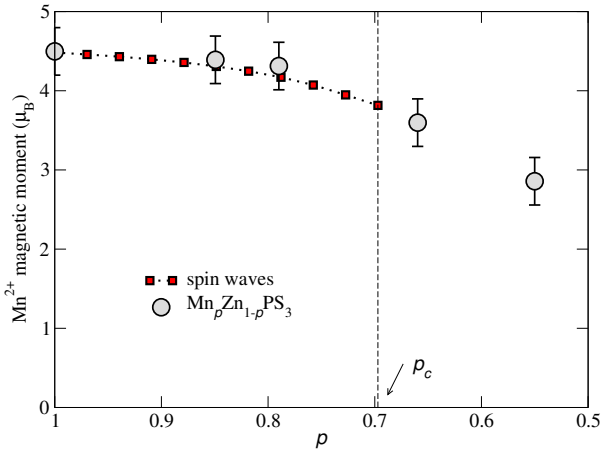

FIG. 8: (color online) Average magnetic moment per magnetic site as function of dilution p. The linear spin wave result for the $S = 5/2$ Heisenberg antiferromagnet in the honeycomb lattice (red squares) is compared with neutron scattering data on $Mn_pZn_{1-p}PS_3$ from Ref. 2 (grey circles).

model. Furthermore, the agreement between experimental and theoretical results even at $p = p_c$, indicates that the primarily effect of second- and third-nearest neighbor interactions is classical. That is, the existence of one largest connected cluster with a finite fraction of spins in the thermodynamic limit is guaranteed by this couplings for $p > p_c$, but the quantum correction to the staggered magnetization density is determined by the smaller first-nearest neighbors clusters belonging to this larger one, at least for $p \gtrsim p_c$. Further investigations are needed to clarify whether this is the correct picture.[39]

b. $Ba(Ni_pMg_{1-p})_2V_2O_8$ The layered compound $BaNi_2V_2O_8$ is a spin $S = 1$ antiferromagnet in a honeycomb lattice. Neutron diffraction experiments have found, in the pure case, an average magnetic moment of $1.55(4)\,\mu_B$ for Ni at 8 K,[19] which is in good agreement with the spin wave result $m \approx 1.48\,\mu_B$. To our knowledge, the magnetic moment has not yet been measured for the diluted compound. Nevertheless, the available magnetic susceptibility measurements on $Ba(Ni_pMg_{1-p})_2V_2O_8$ for dilutions in the range $0.84 \leq p \leq 1$, show that the Néel temperature is strongly dependent on the amount of dilution.[19] For the highest diluted sample ($p = 0.84$) a reduction of almost 70% relative to the undiluted Néel temperature was found. It would be interesting to know whether the suppression of antiferromagnetic LRO by nonmagnetic impurities will occur at the classical percolation transition $p_c \simeq 0.7$, as predicted in our calculations.

D. Néel Temperature

The Néel temperature of both $Mn_pZn_{1-p}PS_3$ and $Ba(Ni_pMg_{1-p})_2V_2O_8$ shows a linear suppression with increasing dilution $1 - p$,[2,19] a feature that is also seen in (quasi-2D) diluted Heisenberg antiferromagnets with square lattice.[40–42]

Within the linear spin wave theory developed in Secs. II and III for diluted antiferromagnetic systems the finite temperature staggered magnetization is given by

$$\begin{aligned} M_z^{\rm stagg}(T) &= \left\langle \sum_{i\in A} S_i^{a,z} - \sum_{i\in B} S_i^{b,z} \right\rangle \\ &= N_{\rm c}\big(S - \delta m_z - \delta m_z^T(T)\big), \end{aligned} \tag{83}$$

where δm_z is the zero-temperature correction to the staggered magnetization defined in Eq. (59), and $\delta m_z^T(T)$ is the thermal correction

$$\delta m_z^T(T) = \sum_{n=1}^{N_a} \delta m_z^{(n,\alpha)} n_B(\omega_n^{(\alpha)}) + \sum_{n=1}^{N_b} \delta m_z^{(n,\beta)} n_B(\omega_n^{(\beta)}), \tag{84}$$

with generalized $\delta m_z^{(n,\alpha)}$ and $\delta m_z^{(n,\beta)}$,

$$\delta m_z^{(n,\alpha)} = \frac{1}{N_{\rm c}} \left(\sum_{i\in A} |u_{ni}|^2 + \sum_{i\in B} |v_{ni}|^2 \right), \tag{85}$$

$$\delta m_z^{(n,\beta)} = \frac{1}{N_{\rm c}} \left(\sum_{i\in A} |w_{ni}|^2 + \sum_{i\in B} |x_{ni}|^2 \right), \tag{86}$$

and $n_B(\omega) = (e^{\omega/k_BT} - 1)^{-1}$ is the Bose distribution function. In the thermodynamic limit the averaged over disorder staggered magnetization density can be expressed as

$$m_{\rm av}(p, T, L \to \infty) = m_{\rm cl} m_{\rm qm}(T), \tag{87}$$

where $m_{\rm cl}$ is the classical factor defined in Eq. (76), and $m_{\rm qm}(T)$ is the temperature dependent quantum mechanical factor,

$$m_{\rm qm}(T) = S - \delta m_z^{\infty} - \delta m_z^{T,L\to\infty}(T). \tag{88}$$

In the undiluted case the thermal correction $\delta m_z^T(p = 1, T)$ can be expressed as

$$\delta m_z^{T,L}(p = 1, T) = \frac{1}{N_a + N_b} \sum_{\mathbf{k}} \frac{h_a}{\sqrt{h_a^2 - |\phi_{\mathbf{k}}|^2}} n_B(\omega_{\mathbf{k}}), \tag{89}$$

with $\omega_{\mathbf{k}}$ as in Eq. (24), and $\phi_{\mathbf{k}}$ given by Eq. (22). The summation in $\mathbf{k}$ is done in the first Brillouin zone of sublattice A or B, and can be replaced by an integration when $L \to \infty$. When $h_a = 1$ the spin wave dispersion behaves as $\omega_{\mathbf{k}} \propto k$ in the long wave length limit, similarly to the square lattice case. As a consequence the thermal correction to the staggered magnetization develops a logarithmic divergence, which signals the well known suppression of LRO at $T > 0$ in the 2D isotropic Heisenberg model.

Therefore, if LRO is present up to $T_N \neq 0$, either a magnetic anisotropy h_a or a finite interplanar exchange

$J_\perp$ (or both) must be present. If the former is the dominant effect T_N can be calculated using the mean-field like equation[58]

$$m_{\rm qm}(T_N) = 0. \tag{90}$$

In the latter the transition should occur when the interplanar coupling is strong enough to stabilize the LRO in comparison with thermal fluctuations:

$$J_\perp m^2_{\rm qm}(p, T=0)\frac{\xi^2(p,T_N)}{A/2} \approx k_B T_N, \tag{91}$$

The parameter $\xi(p,T)$ is the inplane correlation length, which characterizes the spin fluctuations of a layered system in a paramagnetic phase. The area of a hexagon of side c is given by $A = c^2 3\sqrt{3}/2$. The correlation length can be calculated in the context of the modified spin wave theory,[43] and in the non-diluted ($p = 1$) case it is exponentially divergent with $1/T$ as $T \to 0$. The mean field picture which leads to Eq. (91) was proposed in Ref. 7, and gives a good description of the variation of $T_N(p)/T_N(0)$ with dilution $1-p$ in a variety of layered compounds with square lattice.

In the case of $MnPS_3$ a small gap of magnitude $\Delta E = 0.5$ meV was found in the spin wave energy at the the Brillouin zone center.[16] This energy gap can be explained by either a single-ion anisotropy or a dipole coupling, being modeled here by a small magnetic anisotropy $h_a > 1$. From the spin wave dispersion (24) it is found that $h_a \approx 1.004$ is needed to obtain $\Delta E = 0.5$ meV (a nearest-neighbor exchange of magnitude $J = 0.8$ meV was used[16]). We remark that such a small magnetic anisotropy has no effect in the conclusions we have made so far based in the isotropic Heisenberg model ($h_a = 1$). As an example, the the average magnetic moment on the Mn atoms given by spin-wave theory is $m \approx 4.48\,\mu_B$ for $h_a = 1$ and $m \approx 4.55\,\mu_B$ for $h_a = 1.004$, both in excellent agreement with the experimental value $4.5(2)\,\mu_B$ at 3.5 K.[2] Inserting this value of h_a into Eq. (89) we obtain $T_N \approx 70$ K as a solution of Eq. (90), in agreement with the measured value $T_N = 78$ K.[14]

Nevertheless a finite interplanar exchange of magnitude $J_\perp = 0.0019(2)$ meV is also present in the $MnPS_3$ compound.[16] With $\xi(p=1, T_N = 78\ {\rm K}) = 27.5$ Å measured by neutron scattering,[44] and $c = 3.5$ Å,[45] we obtain from the mean field equation (91) $T_N \approx 6$ K. This small value of T_N is an indication that the effect of the interplanar coupling is not as important as the magnetic anisotropy in stabilizing the LRO. Therefore we use Eq. (90) to study the effect of dilution on $T_N(p)$. The thermal correction δm_z^T defined by Eq. (84) is computed via recursion method (see Subsect. III F), noting that it can be expressed as

$$\delta m_z^T(T) = \int_0^\infty dE n_B(E) K(E), \tag{92}$$

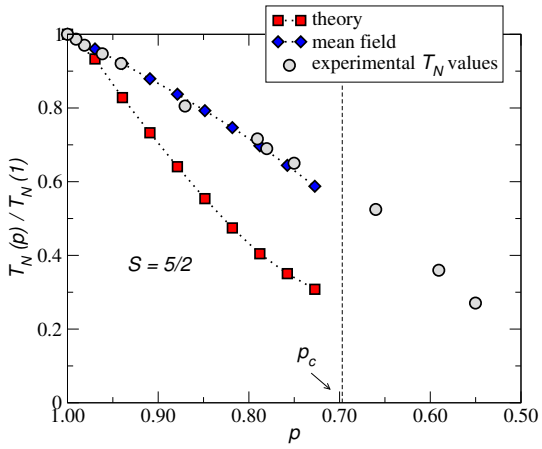

FIG. 9: (color online) $T_N(p)/T_N(0)$ vs p for $S = 5/2$. Shown are the results obtained by numerically solving Eq. (90) with δm_z^T computed applying the recursion method to systems with $L = 128$ and averaging over 200 to 400 disorder realizations (squares), the mean-field result of Eq. (94) (diamonds), and experimental results on $Mn_pZn_{1-p}PS_3$ from Ref. 2 (circles).

where the kernel $K(E)$ is given by

$$K(E) = -\frac{1}{N_{\rm c}}\frac{1}{\pi}{\rm Im}\Bigg[\sum_{i\in A} G^{aa}_{ii}(E+i0^+) + \sum_{i\in B} G^{bb}_{ii}(E+i0^+) + \sum_{i\in A} G^{aa}_{ii}(-E+i0^+) + \sum_{i\in B} G^{bb}_{ii}(-E+i0^+)\Bigg]. \tag{93}$$

It is worth mentioning that with the recursion method δm_z^T can be computed with the same precision (limited by the linear size $L = 128$ of the sample) from the undiluted limit $p = 1$ to the percolation threshold $p = p_{\rm c}$.

The result of numerically solving Eq. (90)—with δm_z^T computed by applying the recursion method to systems with $L = 128$ and averaging over 200 to 400 disorder realizations—is shown in Fig. 9. Also shown are the results of magnetometry measurements on $Mn_pZn_{1-p}PS_3$ from Ref. 2. The difference between the theoretical results and experimental values suggests that in opposition to the magnetic moment at zero temperature (see Fig. 8) the effect of second- and third-nearest-neighbor couplings should be included to obtain a quantitatively correct Néel temperature as dilution is increased. An estimation of $T_N(p)/T_N(1)$ can as well be obtained by standard mean-field theory, $T_N^{MF} = \frac{2}{3}JzS(S+1)$.[46] Replacing S by the zero temperature staggered magnetization density $m_{av}(p)$ defined in Eq. (75), and assuming that the coordination number decreases linearly with dilution, $z \propto p$, the ratio $T_N(p)/T_N(1)$ is given by

$$\frac{T_N(p)}{T_N(1)} = p\, m_{av}(p)[m_{av}(p)+1]. \tag{94}$$

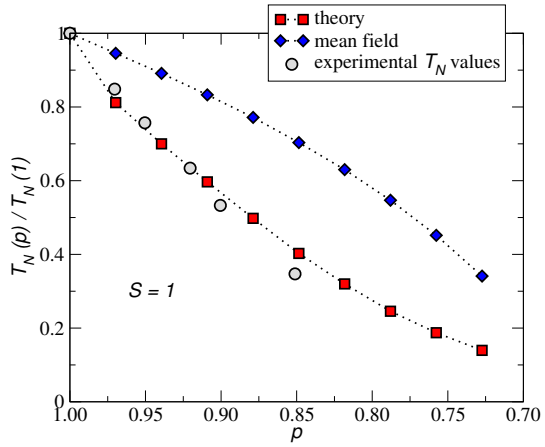

FIG. 10: (color online) $T_N(p)/T_N(0)$ vs p for $S = 1$. Shown are the results obtained by numerically solving Eq. (90) with δm_z^T computed applying the recursion method to systems with $L = 128$ and averaging over 200 to 400 disorder realizations (squares), the mean-field result of Eq. (94) (diamonds), and experimental results on $Ba(Ni_pMg_{1-p})_2V_2O_8$ from Ref. 19 (circles).

In Fig. 9 we show as diamonds the results of Eq. (94). Although this result reproduces the correct dependence on p, it should be stressed that as a mean-field approximation the absolute value of $T_N(p)$ is overestimated.

The effect of dilution on the Néel temperature of $Ba(Ni_pMg_{1-p})_2V_2O_8$ was studied by Rogado *et al.* for dilutions in the range $0.84 \leq p \leq 1$.[19] The few experimental results concerning the magnetic properties of $BaNi_2V_2O_8$ are insufficient to undoubtedly determine the model which better describes the magnetic behaviour of this compound. Although electron-spin resonance measurements seem to be well fitted by a weakly anisotropic Heisenberg model with easy-plane symmetry (XY), *i.e.*, $h_a \lesssim 1$ in Hamiltonian (10), the same results can as well be explained with the isotropic limit of this model.[20] Further experiments would be valuable in determining the nature of the LRO observed in this compound, in particular inelastic neutron scattering from which the spin wave dispersion can be measured. Here we assume that a small gap is present at the Brillouin zone center, and that it can be modeled by a small uniaxial interaction anisotropy, *i.e.*, $h_a \gtrsim 1$ in Hamiltonian (10). In particular $h_a - 1 \approx 10^{-4}$ is needed to get $T_N \approx 50$ K in the undiluted case (a nearest-neighbor exchange of magnitude $J \approx 4$ meV was used).[19]

The $T_N(p)/T_N(1)$ vs p result obtained by numerically solving Eq. (90) for $S = 1$, with δm_z^T computed applying the recursion method to systems with $L = 128$ and averaging over 200 to 400 disorder realizations is shown in Fig. 10 (squares). Also shown are the mean-field result of Eq. (94) (diamonds) and results of magnetic susceptibility data for $Ba(Ni_pMg_{1-p})_2V_2O_8$ (circles) (Ref. 19). The disagreement between the mean-field result (Eq. (94)) and experimental values can be attributed to the small spin $S = 1$ value, which means higher quantum fluctuations and less mean-field like behaviour. The theoretical result (squares) and the experimental values are in reasonable agreement, though it seems to worsen as dilution increases. It should be noted that the spin-wave theory for layered materials is not really adequate at $T \sim T_N$, and when it is applied to the mean-field like Eq. (90) it tends to overestimate the absolute value of the Néel temperature.[47]

E. Density of states

The effect of dilution has a strong impact on the DOS of the system. Since the momentum is no-longer a well defined quantum number the spin waves acquire a finite lifetime.[7] As a consequence, the basis that diagonalizes the problem has a very different energy spectrum, which implies a different DOS.

We have calculated the DOS of the antiferromagnetic Heisenberg model in the linear spin wave approximation for the honeycomb and square lattices in the presence of dilution. The recursion method briefly discussed in Subsect. III F was used to study the variation of the DOS with dilution. The method is valid from the undiluted $p = 1$ limit to the percolation threshold p_c, and enables the access to the whole energy spectrum. The precision limit is set by the linear size L of the system, which we fix here to $L = 128$ both in the honeycomb and square lattices.

In Fig. 11 we show the square lattice DOS at four different values of dilution x. The depletion of the high energy part of the DOS in favor of low energy modes is clearly seen as dilution is increased, in agreement with the results obtained by exact diagonalize smaller systems.[4] The two structures visible at around $E/JS = 2$ and 3, which Mucciolo *et al.*[4] associated with the breaking of the clean-limit magnon branch into three distinct but broad branches, are also evident.

The DOS for the honeycomb lattice is shown in Fig. 12. A decrease in the density of high-frequency states and the proportional increase in the density of low-frequency ones is also clear as dilution increases. This feature can then be viewed as a general effect of the presence of dilution. Structures as those observed in the square lattice case, just below $E/JS = 2$ and 3, are not so easily identified. Nevertheless, a feature of this kind seems to be present just below $E/JS = 2$. To determine whether or not it can be associated to the presence of fractons, as in the square lattice case,[4] a more detailed study is needed, such as the calculation of the dynamical structure factor in the diluted honeycomb lattice.

The effect of moving spectral weight from the top of the band to lower energies due to dilution is accompanied by the appearance of a set of peaks, starting to develop in the high-frequency part of the spectrum for small dilution and extending to the entire band as dilu-

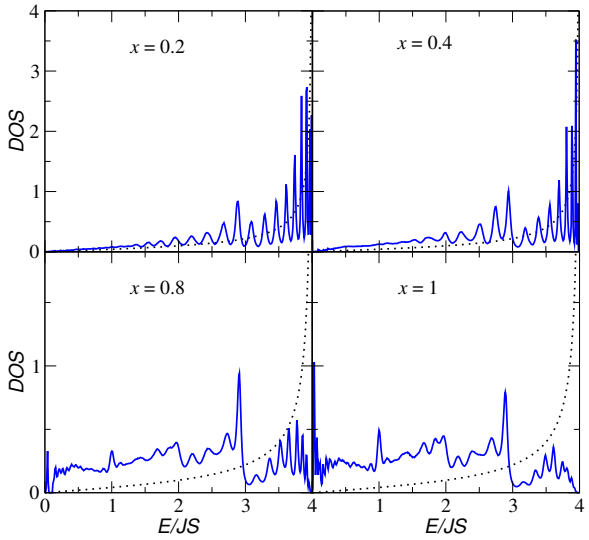

FIG. 11: (color online) DOS of the Heisenberg antiferromagnetic model in the linear spin wave approximation for the square lattice. An energy mesh with spacing 0.01 in units of JS was used. This results were obtained applying the recursion method to systems with $L = 128$, and averaging over 200 to 400 disorder realizations. The dotted line is the clean limit DOS.

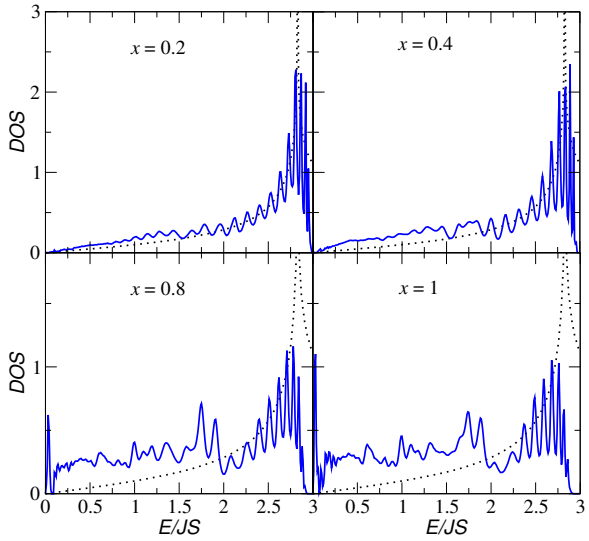

FIG. 12: (color online) DOS of the Heisenberg antiferromagnetic model in the linear spin wave approximation for the honeycomb lattice. An energy mesh with spacing 0.01 in units of JS was used. This results were obtained applying the recursion method to systems with $L = 128$, and averaging over 200 to 400 disorder realizations. The dotted line is the clean limit DOS.

tion increases. There is, however, a particular peak that deserves special attention. This peak can be seen very close to the bottom of the band ($E = 0$) for $x \geq 0.8$ both in the honeycomb and square lattice DOS. Figure 13 is a zoom of the DOS close to $E = 0$ at $x = x_c$. Being present both in the honeycomb and square lattices, though a bit stronger in the former, this peak seems to be a general feature associated with dilution. In fact, it is closely related to the finiteness of the quantum corrections to the staggered magnetization at zero temperature.

As shown by Mucciolo *et al.*[4], the finiteness of the quantum fluctuations reduces to the problem of the convergence of the integral $\int_0^{E_{max}} dE\rho(E)E^{-1}$. In Fig. 13 we show a polynomial fit to the low-energy behaviour of the DOS (red line in the left side of the peak). Although it should be seen as guide to the eyes, we can undoubtedly say that in the low-energy limit the DOS behaves as $\rho(E) \propto E^{\alpha}$ with $\alpha > 1$, and thus the above mentioned integral is convergent. This result is consistent with the existence of an upper bound for the quantum fluctuations in any model with a classically ordered ground state whose Hamiltonian can be mapped onto that of a system of coupled harmonic oscillators, argued by Mucciolo *et al.*.[4] This result also agrees with the FSS results presented in Subsect. III E, where we found finite values for $\delta m_z^{\infty}(x)$. And the fact that $\delta m_z^{\infty}(x_c) > 1/2$ can be attributed to the bad-behaviour of the spin-wave approximation when $\delta m_z \sim S$, as will be shown in the next section.

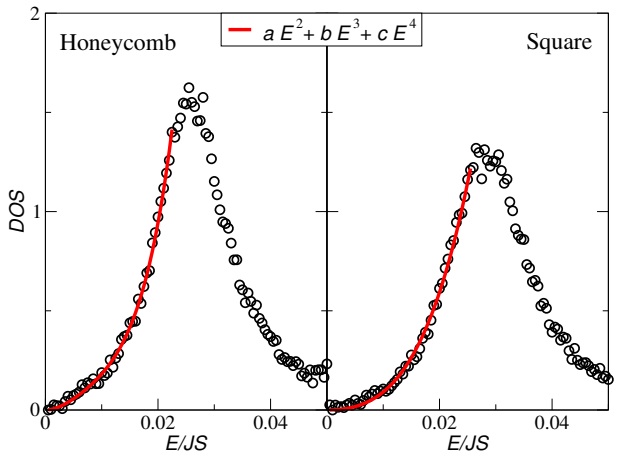

FIG. 13: (color online) Low energy behaviour of the DOS of the Heisenberg antiferromagnetic model in the linear spin wave approximation for the honeycomb (left) and square (right) lattices at $x = x_c$. An energy mesh with spacing 5×10^{-4} in units of JS was used. This results were obtained applying the recursion method to systems with $L = 128$, and averaging over 800 disorder realizations.

F. Quantum Monte Carlo results for $S = 1/2$

We have performed a Monte Carlo study of the $S = 1/2$ quantum Heisenberg antiferromagnet on the site-diluted honeycomb lattice using Stochastic Series Expansion (SSE).[37,48] Unlike the spin wave approach described

in Sects. II and III—which should be understood as an expansion in the relative reduction of the staggered moment $\delta m_z/S$—this technique is exact (up to statistical uncertainties) and well-behaved even when $\delta m_z \sim S$. In particular, the SSE Monte Carlo can access the the small-S, near-percolation regime where the spin wave calculation becomes unreliable.

We have closely followed the procedure outlined in Ref. 5, which treats the site dilution problem on the square lattice. To accelerate convergence, we have taken advantage of the β-doubling scheme described therein: 100 equlibration and 200 sampling sweeps are performed at each temperature with the resulting configuration (an M-element operator list $S_M = [a_1, b_1], \ldots, [a_M, b_M]$) used to generate a high-probability initial configuration at the next lowest temperature ($S_{2M} = [a_1, b_1], \ldots, [a_M, b_M], [a_M, b_M], \ldots, [a_1, b_1]$) according to the cooling schedule $\beta = 2, 4, 8, \ldots, 2048, 4096$.

A refinement to previous work is that we extrapolate the staggered magnetization to the thermodynamic limit using *two* different quantities:

$$m_{\mathrm{qm}} = \lim_{L\to\infty} \left\langle \frac{2}{N_{\mathrm{c}}} \left| \hat{M}_z^{\mathrm{stagg}} \right| \right\rangle_{L,x}, \tag{95a}$$

$$m_{\mathrm{qm}}^2 = \lim_{L\to\infty} \left\langle \frac{3}{N_{\mathrm{c}}^2} \left(\hat{M}_z^{\mathrm{stagg}} \right)^2 \right\rangle_{L,x}. \tag{95b}$$

Here, $\hat{M}_z^{\mathrm{stagg}} = \sum_{i\in A} \hat{S}_i^z - \sum_{i\in B} \hat{S}_i^z$ is the z-projected staggered magetization and m_{qm} is the quantum mechanical factor introduced in Subsect. III E. The notation $\langle \cdot \rangle_{L,x}$ represents an ensemble average over the quantum states of the system and over all configurations of the size-L lattice with dilution x. The site indices in $\hat{M}_z^{\mathrm{stagg}}$ are understood to range over only the largest connected cluster.

Equation (95a), being linear, is analogous to the quantity $S - \delta m_z$ computed via spin wave theory. Equation (95b) is essentially a structure factor and equivalent to Eq. (10) of Ref. 5. The factors 2 and 3 in Eqs. (95) are a consequence of the rotational invariance of the ground state. Their particular values follow from the averages $\int d\hat{\Omega}\, |\hat{\Omega}\cdot\hat{z}| = 4\pi/2$ and $\int d\hat{\Omega}\, (\hat{\Omega}\cdot\hat{z})^2 = 4\pi/3$ where $\hat{\Omega}$ is a vector ranging over the unit sphere. (Such geometric factors are irrelevant to the spin wave case; there the ground state is symmetry-broken by explicit construction.)

As in Ref. 5, we use the straight-forward generalization of the finite-size scaling form for the clean system,[49]

$$\left\langle \frac{2}{N_{\mathrm{c}}} \left| \hat{M}_z^{\mathrm{stagg}} \right| \right\rangle_{L,x}^2 = m_{\mathrm{qm}}^2 + \frac{a_1}{\sqrt{\bar{N}_{\mathrm{c}}}} + \frac{a_2}{\bar{N}_{\mathrm{c}}} + \cdots, \tag{96a}$$

$$\left\langle \frac{3}{N_{\mathrm{c}}^2} \left(\hat{M}_z^{\mathrm{stagg}} \right)^2 \right\rangle_{L,x} = m_{\mathrm{qm}}^2 + \frac{b_1}{\sqrt{\bar{N}_{\mathrm{c}}}} + \frac{b_2}{\bar{N}_{\mathrm{c}}} + \cdots. \tag{96b}$$

[As the discussion in Subsect. IV A makes clear, this converges to $L^{-D/2}$ powerlaw behavior at large L, as in Eq. (77).] Numerical measurements of the two quantities on the left-hand side of Eqs. (96a) and (96b) may be fit to the corresponding functions on the right-hand side either simulaneously—with parameters m_{qm}, $\{a_i\}$, $\{b_i\}$—or separately—with parameters m_{qm}, $\{a_i\}$ and m'_{qm}, $\{b_i\}$. Verifying that $m_{\mathrm{qm}} \approx m'_{\mathrm{qm}}$ serves as a consistency check.

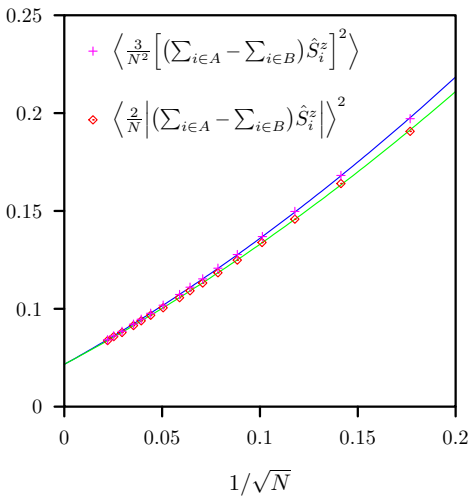

FIG. 14: The staggered magnetization of the undiluted honeycomb lattice ($x = 0$, $N_{\mathrm{c}} = N = 2L^2$) is extrapolated to the thermodynamic limit following Eqs. (96a) and (96b). A simultaneous fit of the two data sets yields the value $m_{\mathrm{av}}(L\to\infty) = 0.2677(6)$.

In the case of the *undiluted* honeycomb lattice (for which $m_{\mathrm{av}}(L\to\infty) \equiv m_{\mathrm{qm}}$), we have simulated lattices up to linear size $L = 32$ (*i.e.*, up to $2\times 32^2 = 2048$ sites). Observables were computed using a bootstrap analysis[50] of 150 bins of 10^5 samples each (1.5×10^6 total Monte Carlo sweeps). Best fits to the data, shown in Fig. 14, give the thermodynamic limit $m_{\mathrm{av}}(L\to\infty) = 0.2677(6)$. This is somewhat smaller than the square lattice value $m_{\mathrm{av}}(L\to\infty) = 0.3070(3)$,[5] a reduction that reflects the larger quantum fluctuations on the less meanfield-like honeycomb lattice.

Note that our value of the staggered magnetization is larger than (but consistent with) an earlier Monte Carlo measurement due to Reger *et al.*[51] (within 1.6 standard deviations). It is also, we believe, considerably more accurate. The Reger group's value of $m_{\mathrm{av}}(L\to\infty) = 0.22(3)$ was computed by extrapolating relatively large Trotter errors ($0.1 < \Delta\tau < 0.2$) to $\Delta\tau \to 0$ and small systems sizes ($4 < L < 8$) to $L\to\infty$. Moveover, their analysis supposes that the inverse temperature $\beta = 10$ is sufficiently cold to extract the ground state properties of the system, which is very likely incorrect.[5]

For the *diluted* honeycomb lattice, we computed the staggered magnetization as an average over 10^5 randomly-generated disorder realizations. Simulations of system sizes up to $\bar{N}_{\mathrm{c}} \approx 2000$ were extrapolated to the thermodynamic limit, as shown in Fig. 15. The figure inset illustrates the dependence of m_{qm} on dilution.

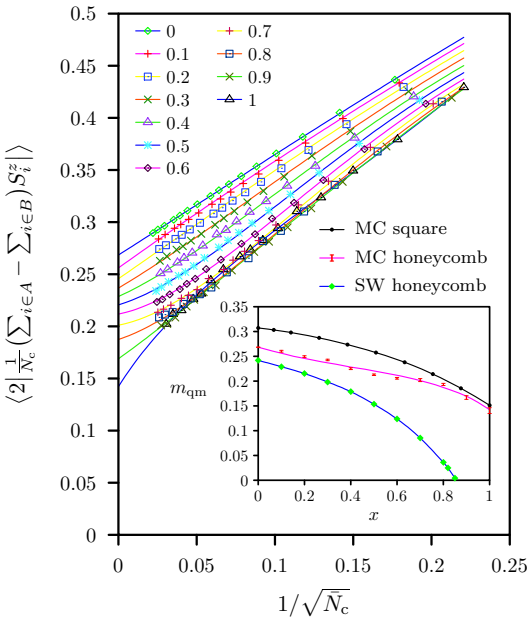

FIG. 15: (color online) The main plot shows an extrapolation to the thermodynamic limit of twice the z-projected staggered magnetization for various dilution levels x (as indicated by the symbols in the upper-left legend). The lines drawn through the data points represent a global fit to Eqs. (96) in which $m_{\rm qm}(x), a_1(x), b_1(x), \ldots$ are treated as powerseries in x and varied. The resulting function $m_{\rm qm}(x)$ appears as the solid (pink) line in the figure inset alongside Monte Carlo results for the square lattice (from Ref. 5) and spinwave results for the honeycomb lattice. The (red) errorbars indicate the values of $m_{\rm qm}$ extrapolated from each fixed-x dataset taken individually.

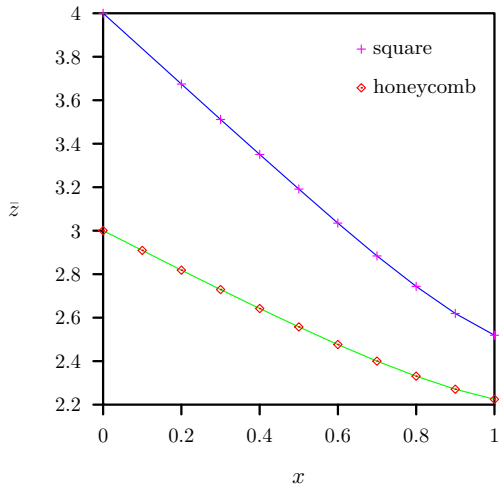

FIG. 16: The disorder-averaged coordination number $\bar{z}(x)$ is plotted as a function of dilution level for infinite square and honeycomb lattices. The difference between the two lattice types narrows as $x \to 1$. The undiluted square lattice is 33% more coordinated than the honeycomb lattice. At percolation, it is only 12% more so.

In contrast to the spinwave prediction, we find that LRO persists right up to the classical percolation threshold. The magnitude of the staggered magnetization decreases with dilution but does not vanish: $m_{\rm qm} = 0.139(6)$ at $x = 1$, which represents a roughly 50% reduction in magnetic moment over the undiluted ($x = 0$) lattice. This is comparable to the effect seen in the square lattice where $m_{\rm qm}(0) = 0.3070(3)$ falls to $m_{\rm qm}(1) = 0.150(2)$.

We observe that the square- and honeycomb-lattice values of $m_{\rm qm}$ are remarkably close in the vicinity of $x = 1$. The likely explanation is that the percolating clusters—retaining little of the structure of their undiluted parent lattice—are themselves quite similar. Both have fractal dimension $D = 91/48$ and a similar nearest neighbour count: with increasing site dilution, the average coordination number goes from $\bar{z}^{\rm hc}(0) = 3$ and $\bar{z}^{\rm sq}(0) = 4$ to $\bar{z}^{\rm hc}(1) = 2.22$ and $\bar{z}^{\rm sq}(1) = 2.52$; see Fig. 16. The Monte Carlo results are consistent with our understanding that the quantum fluctuations disrupt the LRO in inverse proportion to the number of nearest neighbours contributing to the local staggered mean field at each site.

V. SUMMARY AND CONCLUDING REMARKS

In this work we studied the magnetic properties for diluted Heisenberg models in the honeycomb lattice. Refined results for the density of states in the square lattice case were also reported. We have shown that spin wave theory in diluted lattices is quite successful in describing the magnetic properties of $S > 1/2$ systems. On the other hand, for $S = 1/2$, spin wave theory breaks down and one has to approach the problem using a Monte Carlo method. Contrary to the linear spin wave method the, the Monte Carlo method does not allow for the determination of the density of states. Having the advantage of being rotational invariant by construction, the Monte Carlo method does not face the problem of the existence of zero energy modes. We have discussed in detail what is the physics associated with these modes. In the thermodynamic limit they play the role of Goldstone modes, trying to restore the rotational symmetry of the problem, explicitly broken by the spin wave approximation. We have shown that in a numerical study these modes can not be included in the calculation of operator averages, if sensible physical results are to be obtained. This is because these modes were already used in the construction of the broken symmetry state, as was first discussed by P. W. Anderson in his seminal paper on spin waves in non-diluted lattices.[28]

Our approach allows us to compute both the staggered

magnetization and the Néel temperature as function of the dilution concentration. In particular, the combination of spin wave analysis and the recursion method allows for the calculation of physical quantities virtually in the thermodynamic limit. This possibility was not used before in similar studies on the square lattice.

We have used our results to explain the experimental data of two Heisenberg honeycomb systems: $Mn_pZn_{1-p}PS_3$ (a diluted $S = 5/2$ system) and $Ba(Ni_pMg_{1-p})_2V_2O_8$ (a diluted $S = 1$ system). In the first case, the available experimental and theoretical studies in the non-diluted regime suggest that second- and third-nearest-neighbor interactions play a role on the physical properties of the system. This can be seen from the fact that the measured magnetic moment of the samples is finite beyond the classical site-dilution percolation threshold. Our calculation suggests, however, that at low temperatures and for $p > p_c$ the magnetic moment of these samples can be accounted for on the basis of a single nearest-neighbor coupling. On the other hand, the calculation of the Néel temperature using a single nearest-neighbor coupling is underestimated, as it should indeed be case based on the fact that the magnetic order close to the Néel temperature should have a measurable contribution from the other couplings, which are not much smaller than the first nearest-neighbor coupling (the Néel temperature for this system using second- and third-nearest-neighbor interactions will be studied in a future publication). Simple calculations based on simple (Ising like) mean filed theories, on the other hand, are very much insensitive, by construction, to the microscopic details of the system. Therefore, and as long as quantum fluctuations are not important, a good agreement with the experimental data should be obtained. This is the case for $Mn_pZn_{1-p}PS_3$, but not for $Ba(Ni_pMg_{1-p})_2V_2O_8$ since its much smaller spin brings about the contributions of quantum fluctuations. In the case of the system $Ba(Ni_pMg_{1-p})_2V_2O_8$, there are, unfortunately, no measurement of its magnetic moment in the diluted phase, however, the Néel temperature as function of dilution is known from thermodynamic measurements. Our results show that in this case, most likely, only the first-nearest-neighbor coupling (and a very small magnetic anisotropy) are needed to describe the behavior of the Néel temperature upon dilution. It would be important if further investigations on this system could be performed in the future.

Acknowledgements

Some of the understanding presented in this paper on the physics of the zero modes reflects a number of enlightening discussions with J. B. M. Lopes dos Santos, for which the authors are grateful. We thank A. H. Castro Neto for illuminating conversations of the physics of the 2D antiferromagnet in a square lattice. E.V.C. acknowledges the Quantum Condensed Matter Theory Group at Boston University, Boston, MA, U.S.A., for the hospitality, and the financial support of Fundação para a Ciência e a Tecnologia through Grant Ref. SFRH/BD/13182/2003. N.M.R.P. is thankful to the Quantum Condensed Matter visitors program at Boston University, Boston, MA, U.S.A., to the visitors program at the Max-Planck-Institut für Physik komplexer Systeme, Dresden, Germany, and to Fundação para a Ciência e a Tecnologia for a sabbatical grant. E.V.C., N.M.R.P. and J.L.B.L.S. were additionally financed by FCT and EU through POCTI (QCAIII).

APPENDIX A: DIAGONALIZATION OF $H_{\mathbf{k}=\mathbf{0}}$

The $\mathbf{k} = \mathbf{0}$ term in Hamiltonian (21) can be expressed as

$$H_{\mathbf{0}} = JSz\left(h_a(a_{\mathbf{0}}a_{\mathbf{0}}^\dagger + b_{\mathbf{0}}^\dagger b_{\mathbf{0}}) + a_{\mathbf{0}}b_{\mathbf{0}} + b_{\mathbf{0}}^\dagger a_{\mathbf{0}}^\dagger\right). \quad \text{(A1)}$$

This is a standard bilinear model with two coupled modes, which is straightforwardly diagonalized through a Bogoliubov-Valatin transformation (Eq. (25)) when $h_a > 1$. In the isotropic $h_a = 1$ case it has an infinite number of eigenstates with a continuum energy spectrum.

Let us define the following canonical transformation,

$$a_{\mathbf{0}} = \hat{q}_1 + i\hat{p}_1\,, \quad \text{(A2)}$$

$$b_{\mathbf{0}} = \hat{q}_2 + i\hat{p}_2\,. \quad \text{(A3)}$$

We use the *hat* notation to distinguish the operators from their eigenvalues. The new generalized "position" $\hat{q}$ and "momentum" $\hat{p}$ operators satisfy the usual commutation relations:

$$\left[a_{\mathbf{0}}, a_{\mathbf{0}}^\dagger\right] = 1 \quad \Longrightarrow \quad \left[\hat{q}_1, \hat{p}_1\right] = \frac{i}{2}\,; \quad \text{(A4)}$$

$$\left[b_{\mathbf{0}}, b_{\mathbf{0}}^\dagger\right] = 1 \quad \Longrightarrow \quad \left[\hat{q}_2, \hat{p}_2\right] = \frac{i}{2}\,. \quad \text{(A5)}$$

After simple algebra we find that the $h_a = 1$ Hamiltonian (A1) can be written in terms of the new operators $\hat{q}$'s and $\hat{p}$'s as

$$H_{\mathbf{0}} = JSz\left[(\hat{q}_1 + \hat{q}_2)^2 + (\hat{p}_1 - \hat{p}_2)^2\right]. \quad \text{(A6)}$$

The variables $\hat{q}_1 + \hat{q}_2$ and $\hat{p}_1 - \hat{p}_2$ can be interpreted as the center of mass position and the relative momentum, respectively, of a two particle system, therefore commuting with each other

$$[\hat{q}_1 + \hat{q}_2,\, \hat{p}_1 - \hat{p}_2] = \frac{i}{2} - \frac{i}{2} = 0. \quad \text{(A7)}$$

Thus the eigenfunctions of Hamiltonian (A1) are given in as products of the eigenstates of the operator $\hat{q}_1 + \hat{q}_2$ with eigenstates of the operator $\hat{p}_1 - \hat{p}_2$,

$$\Psi_{Q,P}(q_1, q_2) = \delta(q_1 + q_2 - Q)e^{i\frac{P}{2}(q_1 - q_2)}, \quad \text{(A8)}$$

and the aforementioned continuum spectrum is given by

$$E_{Q,P} = JSz(Q^2 + P^2). \quad \text{(A9)}$$

APPENDIX B: ANDERSON BROKEN SYMMETRY ANALYSIS

In this appendix we closely follow the ideas developed by P. W. Anderson[28] to show that the ground state of an antiferromagnet should display broken spin rotational symmetry, even in the absence of any anisotropy.

As was shown in Appendix A the operators $\hat{q}_1+\hat{q}_2$ and $\hat{p}_1-\hat{p}_2$ are constants of the motion in a system described by the isotropic Hamiltonian (A1), having well defined expectation values with zero dispersion. From definitions (A2) and (A3), and Eqs. (20) and (9), it can be easily seen that

$$\hat{q}_1+\hat{q}_2=\frac{1}{\sqrt{2SN_a}}S^x_{\rm tot}\,, \tag{B1}$$

$$\hat{p}_1-\hat{p}_2=\frac{1}{\sqrt{2SN_a}}S^y_{\rm tot}\,, \tag{B2}$$

which explains the constant of motion character of the $\hat{q}_1+\hat{q}_2$ and $\hat{p}_1-\hat{p}_2$ operators ($\mathbf{S}_{\rm tot}$ is a constant of motion of the original Heisenberg model). The uncertainty relation ensures us that their canonical conjugates counterparts will have divergent dispersion. As for Eq. (B1) and (B2) it is not difficult to show that the canonical conjugates of $\hat{p}_1-\hat{p}_2$ and $\hat{q}_1+\hat{q}_2$ are, respectively,

$$\hat{q}_1-\hat{q}_2=\frac{1}{\sqrt{2SN_a}}\left(\sum_{i\in A}S^{a,x}_i-\sum_{i\in B}S^{b,x}_i\right), \tag{B3}$$

$$\hat{p}_1+\hat{p}_2=\frac{1}{\sqrt{2SN_a}}\left(\sum_{i\in A}S^{a,y}_i-\sum_{i\in B}S^{b,y}_i\right). \tag{B4}$$

We want to know how much energy is needed to form a wave packet with states (A8) (above the ground state), such as the expectation values of operators $\hat{q}_1-\hat{q}_2$ and $\hat{p}_1+\hat{p}_2$ have finite dispersion. Let us limit the fluctuations of the expectation value $\langle\hat{q}_1-\hat{q}_2\rangle$ to the range $\Delta_{\hat{q}_1-\hat{q}_2}$. From the uncertainty relation the expectation value of $\hat{p}_1-\hat{p}_2$ must now have a nonzero dispersion, whose magnitude is given by

$$\Delta_{\hat{p}_1-\hat{p}_2}\approx\frac{1}{2\Delta_{\hat{q}_1-\hat{q}_2}}\,. \tag{B5}$$

Thus, to limit $\langle\hat{q}_1-\hat{q}_2\rangle$ to the range $\Delta_{\hat{q}_1-\hat{q}_2}$ we need

$$E_{lim}\simeq\frac{JSz}{4\Delta^2_{\hat{q}_1-\hat{q}_2}}\,, \tag{B6}$$

relatively to the ground state energy. Analogously, to limit $\langle\hat{p}_1+\hat{p}_2\rangle$ to the range $\Delta_{\hat{p}_1+\hat{p}_2}$ we need

$$E_{lim}\simeq\frac{JSz}{4\Delta^2_{\hat{p}_1+\hat{p}_2}}\,. \tag{B7}$$

Defining the the mean square amplitudes of the quantities (62) and (63),

$$\sigma^2_x=\frac{1}{(2N_a)^2}\left\langle\left(\sum_{i\in A}S^{a,x}_i-\sum_{i\in B}S^{b,x}_i\right)^2\right\rangle, \tag{B8}$$

$$\sigma^2_y=\frac{1}{(2N_a)^2}\left\langle\left(\sum_{i\in A}S^{a,y}_i-\sum_{i\in B}S^{b,y}_i\right)^2\right\rangle, \tag{B9}$$

we find from (B3) and (B4) that

$$\Delta^2_{\hat{q}_1-\hat{q}_2}=\frac{2N_a}{S}\sigma^2_x\,, \tag{B10}$$

$$\Delta^2_{\hat{p}_1+\hat{p}_2}=\frac{2N_a}{S}\sigma^2_y\,, \tag{B11}$$

(note that $\hat{q}_1-\hat{q}_2$ and $\hat{p}_1+\hat{p}_2$ have zero expectation value). Inserting (B10) and (B11) in Eqs. (B6) and (B7) it can be seen that to limit σ_x or σ_y to a finite value we only need an excess energy of magnitude $1/N_a$, and hence negligible in the thermodynamic limit. As pointed out by Anderson, we can even limit σ_x or σ_y to values of magnitude $1/N_a^{\frac{1}{2}+\alpha}$, with $\alpha>0$, requiring no energy when $N_a\to\infty$.

[1] O. P. Vajk, P. K. Mang, M. Greven, P. M. Gehring, and J. W. Lynn, Science **295**, 1691 (2002).
[2] D. J. Goossens, A. J. Studer, S. J. Kennedy, and T. J. Hicks, J. Phys.: Condens. Matter **12**, 4233 (2000).
[3] A. L. Chernyshev, Y. C. Chen, and A. H. C. Neto, Phys. Rev. Lett. **87**, 067209 (2001).
[4] E. R. Mucciolo, A. H. C. Neto, and C. Chamon, Phys. Rev. B **69**, 214424 (2004).
[5] A. W. Sandvik, Phys. Rev. B **66**, 024418 (2002).
[6] S. W. Cheong, A. S. Cooper, L. W. Rupp, B. Batlogg, J. D. Thompson, and Z. Fisk, Phys. Rev. B **44**, 9739 (1991).
[7] A. L. Chernyshev, Y. C. Chen, and A. H. C. Neto, Phys. Rev. B **65**, 104407 (2002).
[8] N. M. R. Peres, J. Phys.: Condens. Matter **15**, 7271 (2003).
[9] N. M. R. Peres and M. A. N. Araújo, Phys. Stat. Sol. B **236**, 523 (2003).
[10] N. M. R. Peres and M. A. N. Araújo, Phys. Rev. B **65** (2002).
[11] P. Sengupta, R. T. Scalettar, and R. R. P. Singh, Phys. Rev. B **66** (2002).
[12] I. Spremo, F. Schuetz, P. Kopietz, V. Pashchenko, B. Wolf, M. Lang, J. W. Bats, C. Hu, and M. U. Schmidt, cond-mat/0505425.

[13] G. L. Flem, R. Brec, G. Ouvard, A. Louisy, and P. Segransan, J. Phys. Chem. Solids **43**, 455 (1982).
[14] K. Kurosawa, S. Saito, and Y. Yamaguchi, J. Phys. Soc. Jpn. **52**, 3919 (1983).
[15] P. A. Joy and S. Vasudevan, Phys. Rev. B **46**, 5425 (1992).
[16] A. R. Wildes, B. Roessli, B. Lebech, and K. W. Godfrey, J. Phys.: Condens. Matter **10**, 6417 (1998).
[17] N. Chandrasekharan and S. Vasudevan, Phys. Rev. B **54**, 14903 (1996).
[18] D. J. Goossens and T. J. Hicks, J. Phys.: Condens. Matter **10**, 7643 (1998).
[19] N. Rogado, Q. Huang, J. W. Lynn, A. P. Ramirez, D. Huse, and R. J. Cava, Phys. Rev. B **65**, 144443 (2002).
[20] M. Heinrich, H. K. Von Nidda, A. Loidl, N. Rogado, and R. J. Cava, Phys. Rev. Lett. **91** (2003).
[21] P. Zhou and J. E. Drumheller, J. Appl. Phys. **69**, 5804 (1991).
[22] P. F. De Chatel, J. Chadwick, A. M. Mulders, and T. J. Hicks, Physica B **344**, 117 (2004).
[23] T. Holstein and H. Primakoff, Phys. Rev. **58**, 1098 (1940).
[24] N. M. R. Peres, M. A. N. Araújo, and D. Bozi, Phys. Rev. B **70**, 195122 (2004).
[25] J. H. P. Colpa, Physica A **93**, 327 (1978).
[26] W. H. Press, S. A. Teukolsky, W. T. Vetterling, and B. P. Flannery, *Numerical Recipes in Fortran 77* (Cambridge University Press, Cambridge, 1992), p. 89, 2nd ed.
[27] P. W. Anderson, *Concepts in Solids* (W. A. Benjamin, Massachusetts, 1963).
[28] P. W. Anderson, Phys. Rev. **85**, 714 (1952).
[29] L. Hulthén, Arkiv Mat. Astron. Fysik **26**, 1 (1938).
[30] P. N. Suding and R. M. Ziff, Phys. Rev. E **60**, 275 (1999).
[31] L. Pietronero and A. Stella, Physica A **170**, 64 (1990).
[32] R. Haydock, in *Solid State Physics*, edited by H. Ehrenreich, F. Seitz, and D. Turnbull (Academic Press, New York, 1980), vol. 35, p. 215.
[33] R. Haerle, R. Haydock, and R. L. Te, Comput. Phys. Commun. **90**, 81 (1995).
[34] E. V. Castro, (to be published).
[35] R. Haydock, Phys. Rev. B **61**, 7953 (2000).
[36] K. S. D. Beach, R. J. Gooding, and F. Marsiglio, Phys. Rev. B **61**, 5147 (2000).
[37] A. W. Sandvik, Phys. Rev. B **56**, 11678 (1997).
[38] D. Stauffer and A. Aharony, *Introduction to Percolation Theory* (Taylor and Francis, London, 1992).
[39] E. V. Castro and N. M. R. Peres, (in preparation).
[40] P. Carretta, A. Rigamonti, and R. Sala, Phys. Rev. B **55**, 3734 (1997).
[41] M. Hucker, V. Kataev, J. Pommer, J. Harrass, A. Hosni, C. Pflitsch, R. Gross, and B. Buchner, Phys. Rev. B **59**, R725 (1999).
[42] K. Takeda, O. Fujita, M. Hitaka, M. Mito, T. Kawae, Y. Higuchi, H. Deguchi, Y. Muraoka, K. Zenmyo, H. Kubo, et al., J. Phys. Soc. Jpn. **69**, 3696 (2000).
[43] M. Takahashi, Phys. Rev. B **40**, 2494 (1989).
[44] H. M. Ronnow, A. R. Wildes, and S. T. Bramwell, Physica B **276**, 676 (2000).
[45] K. Okuda, K. Kurosawa, S. Saito, M. Honda, Z. Yu, and M. Date, J. Phys. Soc. Jpn. **55**, 4456 (1986).
[46] W. Jones and N. H. March, *Theoretical Solid State Physics* (Dover, New York, 1985), vol. 1, p. 367.
[47] V. Y. Irkhin, A. A. Katanin, and M. I. Katsnelson, Phys. Rev. B **60**, 1082 (1999).
[48] A. W. Sandvik, Phys. Rev. B **59**, 14157 (1999).
[49] D. A. Huse, Phys. Rev. B **37**, 2380 (1988).
[50] B. Efron and R. Tibshirani, *An Introduction to the Bootstrap* (Chapman & Hall/CRC, Boca Raton, 1993).
[51] J. D. Reger, J. A. Riera, and A. P. Young, J. Phys.: Condens. Matter **1**, 1855 (1989).
[52] P. L'Ecuyer, Math. Comput. **65**, 203 (1996).
[53] Although degeneracy is removed by disorder, we have to handle it if we want our algorithm to be valid in the undiluted case.
[54] Subroutine DHSEQR already gives the product $\mathbf{Y}^{\dagger}\mathbf{Z}$ instead of $\mathbf{Z}$.
[55] The negligence of normalization doesn't change the conclusions we will arrive. Actually, this modes will be identified with the Goldstone modes of the diluted system, which, as in the clean limit, can have divergent amplitude.
[56] This procedure is a highly inefficient one, because only a small fraction ($\sim$ 6% for $L = 14$) of disordered lattice realization are accepted. Nevertheless, the amount of time spent finding clusters with $N_a = N_b$ is a small percentage ($\sim$ 15% and $\sim$ 6% for $L = 14$ in the *Cholesky decomposition method* and *Bogoliubov-Valatin transformation method*, respectively) of the time consumed by the diagonalization subroutines.
[57] As the simulated lattices have $N = 2 \times L \times L$ sites, and the dilution is achieved generating a random number $r \in [0, 1]$ at each lattice site, we need to be careful with the period of the random number generator when averaging over 10^5 disorder realizations. In this work we have used the maximally equidistributed combined Tausworthe generator,[52] as implemented in the *GNU Scientific Library*. The period of this generator is 2^{88} ($\sim 10^{26}$).
[58] The Néel temperature determined from Eq. (90) for isotropic Heisenberg systems is known to be overestimated. In order to correct for it a self consistent solution of this equation is used, where S is replaced by m_{av}. This procedure, very simple to implement in the undiluted case, since there is an analytical expression available for the magnon spectrum, is much more difficult in our case. We postpone the discussion of this aspect to a latter publication.